Diabetologia (2010) 53:1727–1731
DOI 10.1007/s00125-010-1744-6

SHORT COMMUNICATION

Angiotensin II type 1 receptor-independent beneficial effects of telmisartan on dietary-induced obesity, insulin resistance and fatty liver in mice

X. Rong · Y. Li · K. Ebihara · M. Zhao · J. Naowaboot · T. Kusakabe · K. Kuwahara · M. Murray · K. Nakao

Received: 4 January 2010 / Accepted: 4 March 2010 / Published online: 15 April 2010

Abstract
Aims/hypothesis Evidence suggests that telmisartan, an angiotensin II type 1 receptor (AT1) blocker and peroxisome proliferator-activated receptor-γ partial agonist, has beneficial actions that limit development of the metabolic syndrome and diabetes. However, the role played by AT1 inhibition in metabolic effects elicited by telmisartan remains uncertain. Here we isolated the metabolic effects of telmisartan from AT1 antagonism.
Methods Male *At1a* (also known as *Agtr1a*)-deficient mice were fed a standard diet or 60% high-fat diet; those on high-fat diet were co-administered telmisartan (3 mg kg^{-1} day^{-1} by oral gavage) or vehicle for 12 weeks.
Results In *At1a*-null mice, telmisartan prevented high-fat-diet-induced increases in (1) body weight, epididymal and inguinal white adipose tissue weight, adipocyte size and plasma leptin concentration; (2) plasma glucose and insulin concentrations and HOMA index; and (3) liver weight and triacylglycerol content. Insulin tolerance testing also indicated that telmisartan improved the high-fat-diet-induced reduction of glucose-lowering by insulin.
Conclusions/interpretation The present findings demonstrate beneficial, AT1-independent effects of the AT1 blocker telmisartan on dietary-induced obesity, insulin resistance and fatty liver in animals.

Keywords Angiotensin II type 1 receptor · Fatty liver · Insulin resistance · Obesity · Telmisartan

Abbreviations

ARB	Angiotensin II type 1 receptor blocker
AT1	Angiotensin II type 1 receptor
eWAT	Epididymal white adipose tissue
HFD	High-fat diet
ITT	Insulin tolerance test
iWAT	Inguinal white adipose tissue
KO	Knockout
PPAR	Peroxisome proliferator-activated receptor

Introduction

The metabolic syndrome is a cluster of conditions arising from overnutrition and a sedentary lifestyle. Common components of the metabolic syndrome include abdominal obesity, insulin resistance, hypertension and dyslipidaemia. Additional comorbidities may also be present, such as hepatic steatosis leading to non-alcoholic fatty liver disease, proinflammatory and prothrombotic states, and reproductive disorders [1]. Insulin resistance is the key component of the metabolic syndrome. It precedes and predicts the incidence and development of type 2 diabetes and cardiovascular diseases [2].

It has been suggested that activation of the renin–angiotensin system is a common feature in patients with

Electronic supplementary material The online version of this article (doi:10.1007/s00125-010-1744-6) contains supplementary material, which is available to authorised users.

X. Rong · Y. Li (✉) · K. Ebihara · M. Zhao · J. Naowaboot · T. Kusakabe · K. Kuwahara · K. Nakao
Department of Medicine and Clinical Science,
Kyoto University Graduate School of Medicine,
Kyoto 606-8507, Japan
e-mail: yuhao@kuhp.kyoto-u.ac.jp

M. Murray
Laboratory of Pharmacogenomics, Faculty of Pharmacy,
The University of Sydney,
Sydney, NSW 2006, Australia

obesity/the metabolic syndrome [2]. Indeed, blockade of the renin–angiotensin system has been shown in clinical and experimental studies to improve the metabolic syndrome [2]. Most of the established physiological and pathophysiological effects of angiotensin II appear to be mediated through the angiotensin II type 1 receptor (AT1). Angiotensin II type 1 receptor blockers (ARBs) have been used widely in the clinic as antihypertensive agents. More recently, treatment with some ARBs has been found to improve insulin resistance and to protect against the onset and development of type 2 diabetes in insulin-resistant patients with hypertension [2]. Studies in experimental animals seem to support clinical findings [2]. Thus, although the precise mechanisms have yet to be established, the contribution of AT1 signalling and the beneficial effects of AT1 inhibition in the metabolic syndrome are undoubted.

Telmisartan is a well-established ARB. Recently, it was shown to be a partial agonist of the peroxisome proliferator-activated receptor (PPAR)γ in cultured cells [3, 4] and to activate PPARα in cultured hepatic cells and in liver of wild-type mice fed a high-fat diet (HFD) [5]. Telmisartan has also been reported to improve HFD-induced obesity, insulin resistance and fatty liver in wild-type animals [4, 5]. However, the extent to which AT1 inhibition contributes to the beneficial effects of telmisartan treatment has not yet been established. The present study tests the role of AT1 inhibition in telmisartan-elicited metabolic effects using HFD-fed *Atl a* (also known as *Agtr1a*)-knockout (KO) mice.

Methods

Animals, diet and experimental protocol All animal procedures were in accordance with the Principles of Laboratory Animal Care (http://grants1.nih.gov/grants/olaw/references/phspol.htm) and were approved by the Animal Ethics Committee, Kyoto University, Japan. Mice were housed in a temperature-controlled facility (21±1°C, 55±5% relative humidity) with a 12-h light/dark cycle (three to four mice per cage).

Male C57BL/6J wild-type mice were purchased from Japan SLC (Shizuoka, Japan). Male *Atl a*-KO mice on a C57BL/6J background were generated by methods that have been described previously [6]. Animals (8 weeks of age) were divided into three groups (n=8–10 each): (1) standard diet control (standard diet Tel−); (2) HFD control (HFD Tel−); and (3) HFD telmisartan (HFD Tel+) groups. The animals had free access to water and the standard diet (CLEA, Tokyo, Japan) (Tel− group) or HFD (containing 20% [wt/wt] protein, 20% [wt/wt] carbohydrate and 60% [wt/wt] fat) (D12492; Research Diet, New Brunswick, NJ, USA) (HFD Tel− and HFD Tel+ groups). Animals receiving the HFD were also administered telmisartan (3 mg/kg suspended in 5% (wt/vol.) gum arabic (a gift from Boehringer Ingelheim, Tokyo, Japan) or vehicle by oral gavage once daily (between 11:00 and 12:00 hours) for 12 weeks. Daily (24 h) food intake was estimated from weekly measurements. Systolic BP was measured by a tail-cuff method (MK-2000ST; Muromachi Kikai, Tokyo, Japan) at week 5. Blood samples were collected by retroorbital venous puncture under ether anaesthesia at week 10 in animals in non-fasted and fasted (12 h) states. Insulin tolerance tests (ITT; 0.75 IU/kg, i.p.; Humulin R-Insulin; Eli Lilly, Indianapolis, IN, USA) were conducted after fasting (6 h) at week 11. After animals were weighed at week 12, blood samples were collected again from non-fasted animals. Immediately thereafter animals were killed by prompt dislocation of the neck vertebra. Epididymal white adipose tissue (eWAT), inguinal white adipose tissue (iWAT) and liver were collected and weighed. Gastrocnemius was also collected. Glucose, triacylglycerol and NEFA concentrations were determined colorimetrically (Wako, Osaka, Japan), and insulin and leptin concentrations were analysed by ELISA (Morinaga, Tokyo, Japan). HOMA was calculated by method that has been described previously [7].

A portion of eWAT or liver was fixed with 10% formalin (vol./vol.) and embedded in paraffin. Sections (20 μm) were cut and stained with haematoxylin and eosin for examination of adipose tissue and liver histology (IX-81; Olympus, Tokyo, Japan). The adipocyte cross-sectional area was measured using an image analysing system (KS 400; Carl Zeiss Vision, Eching, Germany).

Data analysis All results are expressed as means ± SEM. Data were analysed by one-way ANOVA. If a difference was detected (F ratio), the Student–Newman–Keuls test was performed to locate the differences between groups. Values of $p<0.05$ were considered to be statistically significant.

Results

Consistent with previous reports [4, 5], we have demonstrated that telmisartan treatment (3 mg/kg) did not affect food intake (Electronic supplementary material [ESM] Fig. 1b), but substantially attenuated HFD-induced obesity (ESM Fig. 1c–h), insulin resistance (ESM Fig. 2a–e) and lipid overaccumulation in liver and skeletal muscle (ESM Fig. 3c–g) in C57BL/6J wild-type mice. In the present study, systolic BP in *Atl a*-KO mice was 75±2.5 mmHg (Fig. 1a), which was lower than in wild-type mice (ESM Fig. 1a); telmisartan did not alter systolic BP in *Atl a*-KO mice.

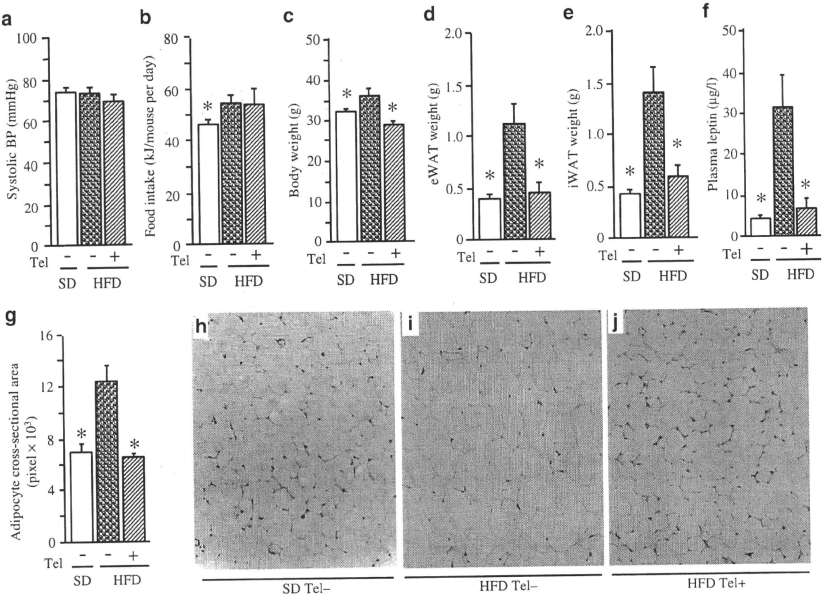

Fig. 1 Systolic BP (**a**), food intake per day (**b**), body weight (**c**), eWAT weight (**d**), iWAT weight (**e**), plasma leptin concentration (**f**), adipocyte cross-sectional area (**g**) and representative images (**h–j**) showing histology of eWAT (haematoxylin and eosin staining, magnification ×200) in male *Atl1a*-KO mice fed standard or HFD for 12 weeks. All values are means ± SEM (n=8–10); *p<0.05 vs HFD control (Tel–). Tel–, vehicle; Tel+, telmisartan 3 mg/kg

HFD feeding significantly increased food intake (Fig. 1b), body weight (Fig. 1c), the weight of eWAT (Fig. 1d) and iWAT (Fig. 1e), adipocyte size (Fig. 1g–i) and plasma leptin concentration (Fig. 1f) in *Atl1a*-KO mice. Telmisartan treatment did not affect food intake, but did ameliorate other variables (Fig. 1c–g, j).

In *Atl1a*-KO mice, HFD feeding increased the fasted plasma glucose (Fig. 2a) and insulin (Fig. 2b) concentrations, and the HOMA index (Fig. 2c) in comparison with those in standard diet-fed *Atl1a*-KO mice. Plasma glucose concentrations after insulin challenge (Fig. 2d) and the glucose AUC during ITT (Fig. 2e) were also increased by HFD treatment. Telmisartan treatment suppressed the HFD-induced increase in all variables.

HFD feeding had no effect on non-fasted and fasted plasma concentrations of triacylglycerol and NEFA (Fig. 2f, g), and on liver weight (Fig. 2h), whereas triacylglycerol content in liver and skeletal muscle was increased against that in standard diet-fed *Atl1a*-KO mice (Fig. 2i, j). Telmisartan treatment decreased liver weight and triacylglycerol content in liver and skeletal muscle. Histological evaluation confirmed that fatty infiltration of the liver was decreased by telmisartan (data not shown). In contrast with the lipid-lowering effects observed in HFD-fed wild-type rats [4] and mice (ESM Fig. 3a, b), telmisartan minimally affected non-fasted and fasted plasma triacylglycerol and NEFA concentrations in HFD-fed *Atl1a*-KO mice.

Discussion

The present study demonstrates that long-term treatment with telmisartan in *Atl1a*-null mice fed a HFD prevents or improves the increase in: (1) body weight, white adipose tissue weight, adipocyte size and plasma leptin concentration; (2) plasma glucose and insulin concentrations, HOMA index, and plasma glucose concentrations and glucose AUC during ITT; and (3) liver weight and triacylglycerol content of the

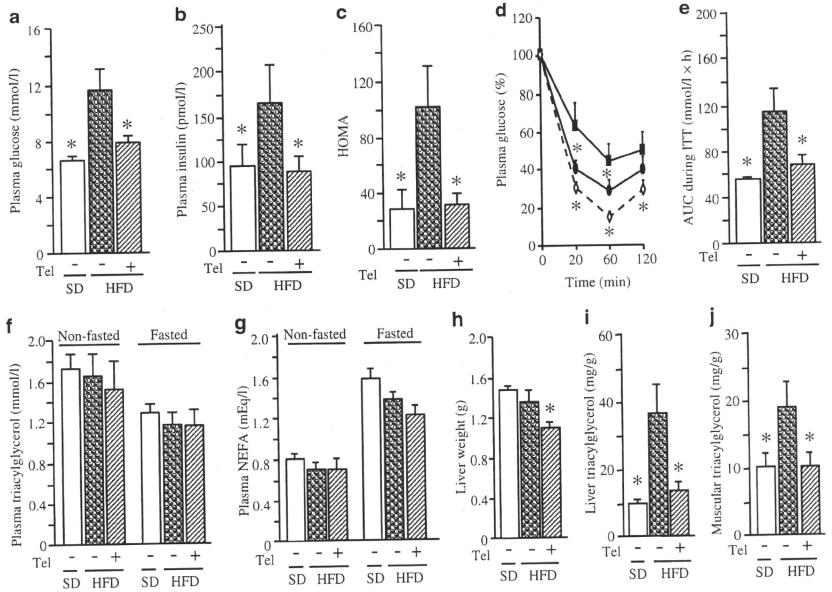

Fig. 2 Fasted (12 h) plasma concentrations of glucose (**a**) and insulin (**b**), HOMA index (**c**), plasma glucose response curve (per cent glucose change) (**d**), plasma glucose AUC following insulin challenge in ITT (Insulin 0.75 IU/kg, i.p.) (**e**), non-fasted and fasted plasma triacylglycerol concentrations (**f**), NEFA concentrations (**g**), liver weight (**h**), and triacylglycerol content of liver and skeletal muscle respectively (**i, j**) in male *Atl a*-KO mice fed a standard diet or HFD. All values are means ± SEM (n=8–10); *p<0.05 vs HFD control (Tel–). Tel–, vehicle; Tel+, telmisartan 3 mg/kg; (**d**) white diamonds, standard diet Tel–; black squares, HFD Tel–; black ovals, HFD Tel+

liver and skeletal muscle. The present findings reveal AT1-independent improvement of dietary-induced obesity, insulin resistance and fatty liver following telmisartan treatment.

Obesity is a well-established metabolic and cardiovascular risk factor. Recent advances have increased our understanding of the cellular mechanisms whereby adiposity induces adverse local and systemic effects. These include lipid accumulation in adipocytes, induction of endoplasmic reticulum and mitochondrial stress, and insulin resistance. Increased adipose tissue mass, especially in the visceral compartment, represents one of the major risk factors for development of type 2 diabetes [8]. We have recently demonstrated that telmisartan treatment improved insulin resistance and fatty liver in A-ZIP/F-1 transgenic mice lacking adipose tissue [7]. These results suggest that telmisartan may elicit its metabolic effects independently of adipose tissue. In the present study, telmisartan treatment attenuated obesity induced by HFD, a finding accompanied by improvement of insulin resistance in wild-type and *Atl a*-KO mice. Thus, the present results suggest that adipose tissue may be an alternative pathway for the insulin-sensitising effect of telmisartan.

On the other hand, an increasing body of evidence indicates that several manifestations of the metabolic syndrome and type 2 diabetes mellitus, including insulin resistance, occur as a result of overaccumulation of lipids in non-adipose tissues, such as liver and skeletal muscle [9]. A decrease in hepatic triacylglycerol pools leads to improved insulin sensitivity [10]. In the present study, HFD-feeding induced excessive lipid accumulation in liver and skeletal muscle, whereas telmisartan treatment ameliorated hepatic steatosis and muscular triacylglycerol deposition in *Atl a*-deficient mice. These results imply that attenuation of diet-induced fatty liver by telmisartan is driven by mechanisms that are independent of AT1. Thus, amelioration of lipid overaccumulation in non-adipose tissues may be an important factor associated with improved insulin action in *Atl a*-null mice following treatment with telmisartan.

In conclusion, the present findings demonstrate for the first time AT1-independent beneficial effects of telmisartan on diet-induced obesity, insulin resistance and fatty liver in mice. Activation of PPARγ might be one potential AT1-independent mechanism of action.

Acknowledgements We thank Y. Yamamoto (Kyoto University) for useful discussions during the preparation of this manuscript and W. Aini for his technical assistance during the project.

Duality of interest The authors declare that there is no duality of interest associated with this manuscript.

References

1. Cornier MA, Dabelea D, Hernandez TL et al (2008) The metabolic syndrome. Endocr Rev 29:777–822
2. Prasad A, Quyyumi AA (2004) Renin–angiotensin system and angiotensin receptor blockers in the metabolic syndrome. Circulation 110:1507–1512
3. Fujimoto M, Masuzaki H, Tanaka T et al (2004) An angiotensin II AT1 receptor antagonist, telmisartan augments glucose uptake and GLUT4 protein expression in 3T3-L1 adipocytes. FEBS Lett 576:492–497
4. Benson SC, Pershadsingh HA, Ho CI et al (2004) Identification of telmisartan as a unique angiotensin II receptor antagonist with selective PPARgamma-modulating activity. Hypertension 43:993–1002
5. Clemenz M, Frost N, Schupp M et al (2008) Liver-specific peroxisome proliferator-activated receptor alpha target gene regulation by the angiotensin type 1 receptor blocker telmisartan. Diabetes 57:1405–1413
6. Li Y, Kishimoto I, Saito Y et al (2002) Guanylyl cyclase-A inhibits angiotensin II type 1A receptor-mediated cardiac remodeling, an endogenous protective mechanism in the heart. Circulation 106:1722–1728
7. Rong X, Li Y, Ebihara K et al (2009) An adipose tissue-independent insulin-sensitizing action of telmisartan: a study in lipodystrophic mice. J Pharmacol Exp Ther 331:1096–1103
8. Bloomgarden ZT (2000) Obesity and diabetes. Diabetes Care 23:1584–1590
9. Unger RH (2002) Lipotoxic diseases. Annu Rev Med 53:319–336
10. Neschen S, Morino K, Hammond LE et al (2005) Prevention of hepatic steatosis and hepatic insulin resistance in mitochondrial acyl-CoA:glycerol-sn-3-phosphate acyltransferase 1 knockout mice. Cell Metab 2:55–65

Establishment of a Novel Ghrelin-Producing Cell Line

Hiroshi Iwakura, Yushu Li, Hiroyuki Ariyasu, Hiroshi Hosoda, Naotetsu Kanamoto, Mika Bando, Go Yamada, Kiminori Hosoda, Kazuwa Nakao, Kenji Kangawa, and Takashi Akamizu

Ghrelin Research Project (H.I., Y.L., H.A., M.B., T.A.), Translational Research Center, and Department of Medicine and Clinical Science, Endocrinology, and Metabolism (N.K., G.Y., K.H., K.N.), Kyoto University Hospital, Kyoto University Graduate School of Medicine, Kyoto 606-8507, Japan; and National Cardiovascular Center Research Institute (H.H., K.K.), Osaka 565-8565, Japan

To establish a tool to study ghrelin production and secretion *in vitro*, we developed a novel ghrelin-producing cell line, MGN3–1 (mouse ghrelinoma 3-1) cells from a gastric ghrelin-producing cell tumor derived from ghrelin-promoter Simian virus 40-T-antigen transgenic mice. MGN3-1 cells preserve three essential characteristics required for the *in vitro* tool for ghrelin research. First, MGN3-1 cells produce a substantial amount of ghrelin at levels approximately 5000 times higher than that observed in TT cells. Second, MGN3-1 cell expressed two key enzymes for acyl modification and maturation of ghrelin, namely ghrelin *O*-acyltransferase for acylation and prohormone convertase 1/3 for maturation and the physiological acyl modification and maturation of ghrelin were confirmed. Third, MGN3-1 cells retain physiological regulation of ghrelin secretion, at least in regard to the suppression by somatostatin and insulin, which is well established in *in vivo* studies. Thus, MGN3-1 cells are the first cell line derived from a gastric ghrelin-producing cell preserving secretion of substantial amounts of ghrelin under physiological regulation. This cell line will be a useful tool for both studying the production and secretion of ghrelin and screening of ghrelin-modulating drugs. (***Endocrinology* 151: 2940–2945, 2010)**

Ghrelin, a stomach-derived hormone, is composed of 28 amino acid residues with unique acyl-modification (1). Plasma ghrelin levels are regulated by acute and chronic energy status: serum levels are increased during a postprandial period and decreased after refeeding (2, 3). Ghrelin levels are low in obese individuals and high in lean people (4, 5). The direct factors regulating ghrelin secretion from ghrelin-producing cells (X/A-like cells), however, are not fully understood.

One method to investigate the direct effect of a specific factor on ghrelin secretion is to use a ghrelin-producing cell line. Ghrelin production has been reported by several cell lines, including TT (6), HL-60, THP-1, SupT1 (7), and HELL (8) cells. All of these cell lines differ completely from endogenous ghrelin-producing cells. TT cells originate from human thyroid medullary cancer, whereas HL-60, SupT1, and HELL cells are leukocyte in origin, with HELL being erythroleukemic line. Although these cell lines may be used to study ghrelin production (9), they are not ideal tools to study the regulation of ghrelin secretion. Therefore, establishment of a cell line originating from ghrelin-producing cells of the stomach would be useful for studying ghrelin production and secretion. Furthermore, it is vital to establish such cell line for studying factors directly affecting ghrelin production and secretion.

In this study, we established a ghrelin-producing cell line from a gastric tumor derived from ghrelin-promoter-Simian virus 40 T-antigen transgenic (GP-Tag Tg) mice.

Materials and Methods

Animals

GP-Tag Tg mice were generated as described previously (10). KSN nude mice were purchased from Shimizu Laboratory Supplies (Kyoto, Japan). Animals were maintained on

ISSN Print 0013-7227 ISSN Online 1945-7170
Printed in U.S.A.

doi: 10.1210/en.2010-0090 Received January 22, 2010. Accepted March 12, 2010.
First Published Online April 7, 2010

Abbreviations: AA, Amino acid; FBS, fetal bovine serum; GOAT, ghrelin *O*-acyltransferase; GP-Tag Tg, ghrelin-promoter-Simian virus 40 T-antigen transgenic; KRB, Krebs-Ringer buffer; PC, prohormone convertase; siRNA, small interfering RNA.

standard rodent food (CE-2, 352 kcal/100 g; Japan CLEA, Tokyo, Japan) on a 12-h light, 12-h dark cycle unless otherwise indicated. All experimental procedures were approved by the Kyoto University Graduate School of Medicine Committee on Animal Research.

Cell culture

A gastric tumor resected from a GP-Tag Tg mouse was minced and digested with the combination of 1.5 mg/ml collagenase type I (Sigma-Aldrich, St. Louis, MO) and 0.5 mg/ml dispase (Roche, Basel, Switzerland) in DMEM (11995-065; Life Technologies, Inc., Carlsbad, CA) supplemented with 10% fetal bovine serum (FBS) at 37 C for 90 min. After washing with PBS, tumor cells were cultured in DMEM supplemented with 10% FBS, 100 U/ml penicillin, and 100 μg/ml streptomycin at 37 C in 10% CO_2. Stromal cells were diminished by serial passage of tumor cells into new dishes 2–3 h after seeding the cells to the first dishes. After several passages of cells in 3-d intervals, the cells were cloned by dilution cloning onto a feeder layer of mitomycin-C-treated embryonic fibroblasts in 96-well microplates.

TT cells were cultured in Ham's F-12K supplemented with 10% FBS at 37 C in 5% CO_2 as described previously (6).

Immunocytochemistry

Cells were cultured in a chamber slide system (Nulge Nunc, Rochester, NY) and then fixed with 10% formalin for 15 min. Formalin-fixed slides were immunostained using the avidin-biotin peroxidase complex method (Vectastain ABC Elite kit; Vector Laboratories, Burlingame, CA) as described previously (11). Slides were incubated with anti-carboxy (C)-terminal ghrelin (amino acid, AA: 13-28) (12) (1:2000 at final dilution), which detects both ghrelin and desacyl-ghrelin, amino N-terminal ghrelin (12) that recognizes the *n*-octanoylated portion of ghrelin (AA: 1–11; 1:5000), antiglucagon (1:500) (Dako, Glostrup, Denmark), antisomatostatin (1:500) (Dako), and antigastrin (1:500) (Dako).

Electron microscope

Electron microscope study was performed as described previously (13). Cell pellets were fixed with 1% glutaraldehyde at 4 C for 2 h. After washing in phosphate buffer, samples were postfixed with 2% OsO_4 at 4 C for 2 h dehydrated with ethanol and embedded in Quetol 812 (Nisshin EM, Tokyo, Japan). Ultrathin sections of samples were cut, stained with uranyl acetate for 15 min followed by lead acetate for 5 min, and then viewed with an H-300 electron microscope (Hitachi, Tokyo, Japan).

Measurements of ghrelin concentrations in cells and culture medium

Cells were detached from dishes in enzyme-free cell dissociation buffer (Life Technologies). After centrifugation, cells were dissolved in PBS and boiled for 5 min. Acetic acid was added to each solution to a final concentration of 1 M. After needle shearing and centrifugation, the cell supernatants were applied to Sep-Pak C18 cartridges (Waters Corp., Milford, MA) preequilibrated with 0.9% saline. Cartridges were washed in saline and 5% CH_3CN/0.1% trifluoroacetic acid and eluted with 60% CH_3CN/0.1% trifluoroacetic acid. Eluates were lyophilized and subjected to ghrelin RIA. To measure ghrelin concentrations in culture medium, the collected culture media were centrifuged, and the resulting supernatants were immediately applied to Sep-Pak C18 cartridges and processed as described above. RIAs were performed using anti-C-terminal ghrelin (AA: 13–28) antiserum (C-RIA), which detects both ghrelin and desacyl-ghrelin, and anti-N-terminal ghrelin (AA: 1–11) antiserum (N-RIA), which detects ghrelin only, as described previously (12, 14).

RT-PCR and quantitative RT-PCR

Total RNA was extracted using a Sepasol-RNA kit (Nacalai Tesque, Kyoto, Japan). Reverse transcription was performed with a high-capacity cDNA reverse transcriptase kit (Applied Biosystems, Foster City, CA). RT-PCR was performed using a GeneAmp 9700 cycler (Applied Biosystems) with Amplitaqgold using appropriate primers (Supplemental Table 1 published on The Endocrine Society's Journals Online web site at http://endo.endojournals.org). Real-time quantitative PCR was performed using an ABI PRISM 7500 sequence detection system (Applied Biosystems) using appropriate primers and TaqMan probes or with Power SybrGreen (Supplemental Table 1). The mRNA expression of each gene was normalized to levels of 18S rRNA.

Western blotting

The molecular size of ghrelin in the medium was determined by tricine SDS-PAGE and Western blot analysis as described previously (10). MGN3-1 cells were seeded in 10-cm dishes (5.0×10^6 cells/dish). Culture media were collected after a 3-d incubation and subjected to HPLC purification and lyophilization as described above. Tricine SDS-PAGE and Western blot analysis were performed as described previously using anti-COOH-terminal ghrelin antibody (1:5000) (10).

Reverse-phase HPLC

MGN3-1 cells were seeded in a six-well dish (5×10^5 cells/well). After a washing in PBS, cells were incubated at 37 C for 4 h in DMEM supplemented with 0.5% BSA. Culture medium was collected and subjected to reverse-phase HPLC as described previously (6).

Small interfering RNA (siRNA)

Synthetic siRNAs and a negative control were purchased from Invitrogen (Carlsbad, CA). Two types of siRNAs specific for ghrelin *O*-acyltransferase (GOAT) were used: GCGCUUCUGUUUAAUUAUCUCUGCA (si1) and AGGAAGUCCAUAGGCUGACCUUCUU (si2). siRNAs were delivered into MGN3-1 cells using Lipofectamine RNAi Max (Invitrogen) according to the protocol provided by the manufacturer. The medium was changed after a 24-h incubation with siRNA. One mM of octanoic acid was added to the medium. Ghrelin levels in the media were measured after additional 6-d incubation.

Transplantation of MGN3-1 cells in nude mice

Eight-week-old male KSN nude mice were sc injected with 1.0×10^7 of MGN3-1 cells dissolved in PBS. Mice were housed individually with continuous access to chow and water. Food intake was measured by subtracting the remaining weight of the chow from that originally presented.

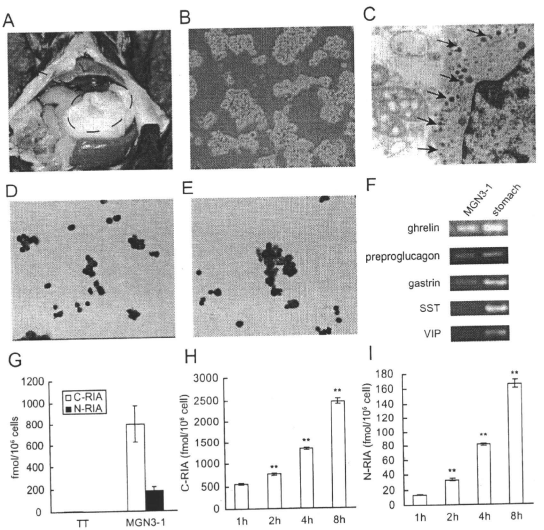

FIG. 1. Establishment of MGN3-1 cells A, Macroscopic findings of a ghrelinoma in a GP-Tag Tg mouse. B and C, Morphology of MGN3-1 cells by optic (B) and electron (C) microscopy. Secretory granules were observed (*arrow*). D and E, MGN3-1 cells were immunostained with anti-C-terminal ghrelin (D) and anti-N-terminal (E) ghrelin antibodies. F, RT-PCR analysis of the expression of mRNAs encoding gastric hormones in MGN3-1 cells. SST, Somatostatin; VIP, vasoactive intestinal polypeptide. G, Ghrelin peptide content determined by C-RIA and N-RIA in TT and MGN3-1 cells. H and I, Time course changes of ghrelin levels in the medium in which MGN3-1 cells were incubated. **, $P < 0.01$ compared with 1 h ($n = 9$).

Measurements of plasma ghrelin concentrations

Plasma samples were collected as reported previously (10). Plasma ghrelin and desacyl ghrelin concentrations were determined using an active ghrelin ELISA kit that recognizes *n*-octanoylated ghrelin and a desacyl ghrelin ELISA kit (both from Mitsubishi Kagaku Iatron, Tokyo, Japan), respectively (15).

Batch incubation study

MGN3-1 cells were seeded and cultured overnight in 12-well plates (7.5×10^5 cells/well). After a washing in PBS, cells were incubated at 37 C for 4 h in DMEM or Krebs-Ringer buffer (KRB) supplemented with 0.5% BSA and the indicated additional reagents (octanoic acid, somatostatin, or insulin) before collecting supernatants. Ghrelin concentrations in the supernatant were measured by RIA as described above. To determine the expression levels of ghrelin and GOAT mRNA, cells were incubated at 37 C for 24 h in DMEM supplemented with 0.5% BSA and the indicated additional reagents.

Statistical analysis

All values were expressed as the means ± SE. The statistical significance of the differences in mean values was assessed by ANOVA with a *post hoc* test (Tukey's test) or Student's *t* test as appropriate. Difference with $P < 0.05$ was considered significant.

Results

Establishment of MGN3-1 cell line

GP-Tag Tg mice (10) develop gastric tumors (Fig. 1A), which produce and secrete ghrelin and preserving the physiological regulation, at least by feeding status, sex difference, and body weights *in vivo*. We established a cell line, MGN3-1 cell, from a gastric tumor derived from a GP-Tag Tg mouse (Fig. 1A). MGN3-1 cells formed round-shaped aggregates that stuck together with moderate adhesion to culture dishes (Fig. 1B). These cells contained secretory granules when observed by electron microscopy (Fig. 1C). MGN3-1 cells exhibited ghrelin-like immunoreactivity by immunocytochemistry using anti-N-terminal, which recognizes ghrelin only, and anti-C-terminal ghrelin, which recognizes both ghrelin and desacyl ghrelin, antibodies (Fig. 1, D and E). We found the production of ghrelin mRNA by MGN3-1 cells using RT-PCR (Fig. 1F). This method also detected low levels of preproglucagon and gastrin mRNA (Fig. 1F) in MGN3-1 cells, whereas immunostaining with antiglucagon and antigastrin antibodies could not detect any expression of these proteins (data not shown). No expression of somatostatin and vasoactive intestinal polypeptide mRNA was observed in MGN3-1 cell (Fig. 1F). MGN3-1 cells contained approximately 140-fold higher levels of total ghrelin (*n*-octanoylated ghrelin plus desacyl ghrelin) measured by C-RIA and approximately 5000-fold higher levels of ghrelin measured by N-RIA than those observed in TT cells (Fig. 1G). The ghrelin levels in the medium were increased time dependently when MGN3-1 cells were incubated in DMEM (Fig. 1, H and I).

Acyl modification and maturation of ghrelin in MGN3-1 cells

MGN3-1 cells expressed GOAT, prohormone convertase (PC) 1/3 and PC2 mRNA (Fig. 2A). The molecular size of ghrelin examined by tricine SDS-PAGE and Western blot analysis in culture medium was consistent with that of mature ghrelin (Fig. 2B). In addition, when the culture

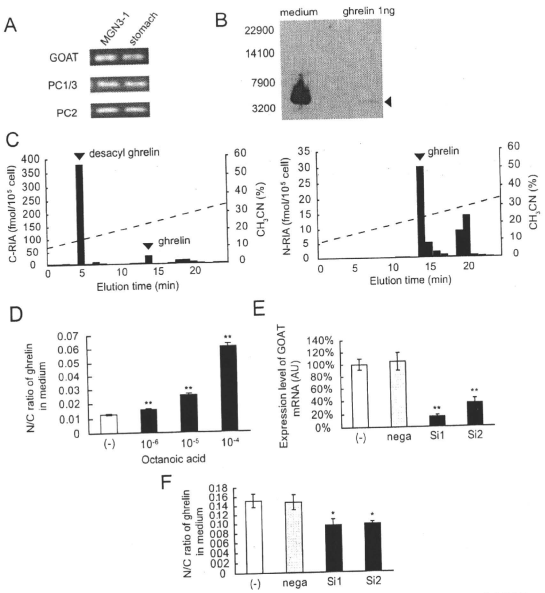

FIG. 2. Acylation and processing of ghrelin in MGN3-1 cells. A, RT-PCR analysis of GOAT, PC1/3, and PC2 mRNA expressions in MGN3-1 cells. B, Western blot analysis of culture medium in which MGN3-1 cells were cultured for 3 d. Rat ghrelin peptide was used as a positive control. C, Representative reverse-phase HPLC profiles of ghrelin immunoreactivity in the medium in which MGN3-1 cells were cultured for 4 h. D, The ratio of N-RIA to C-RIA of ghrelin secreted by MGN3-1 cells incubated for 4 h in KRB supplemented with 0.5% BSA and various concentrations of octanoic acid. **, $P < 0.01$ in comparison with (−) (n = 9). E, GOAT mRNA levels after siRNA treatment of MGN3-1 cells. Two types of siRNA specific for GOAT (Si1 and Si2) and negative control (nega) were introduced into MGN3-1 cell. *, $P < 0.05$, **, $P < 0.01$ in comparison with (−) (n = 7). AU, Arbitrary unit. F, The ratio of N-RIA to C-RIA of ghrelin secreted by MGN3-1 cells after siRNA treatment. *, $P < 0.05$, **, $P < 0.01$ in comparison with (−) (n = 7).

media were subjected to reverse-phase HPLC, the immunoreactive peaks detected by C-RIA and N-RIA were eluted at the positions identical with those of desacyl ghrelin and ghrelin (Fig. 2C). When MGN3-1 cells were incubated in KRB supplemented with 0.5% BSA, addition of octanoic acid to KRB significantly increased the ratio of *n*-octanoylated ghrelin measured by N-RIA to total ghrelin measured by C-RIA (N to C ratio) (Fig. 2D). Specific siRNA1 and siRNA2 treatment decreased GOAT mRNA levels in MGN3-1 cells to 85 and 65% of normal levels, respectively (Fig. 2E). The N to C ratio was significantly decreased by GOAT knockdown (Fig. 2F), indicating that GOAT mediates the acylation of ghrelin in MGN3-1 cells.

Transplantation of MGN3-1 cell to nude mouse

When MGN3-1 cells were injected sc into nude mice, they developed solid tumors (Fig. 3A). Plasma ghrelin and desacyl ghrelin levels were significantly elevated in nude mice 4 wk after MGN3-1 cell injection (Fig. 3, B and C). Mice injected with MGN3-1 cells exhibited significantly higher food intake in comparison with controls (PBS *vs.* cell: 21.4 ± 0.5 *vs.* 23.3 ± 0.7 g/wk, $P < 0.05$) 4 wk after injection (Fig. 3C).

The effect of somatostatin and insulin on ghrelin secretion and expression *in vitro*

MGN3-1 cells expressed the mRNAs encoding multiple somatostatin receptors, primarily type 2 and 5 with lower levels of type 3 and 4 (Fig. 4A. When somatostatin was added to culture media, ghrelin secretion was suppressed in a dose-dependent manner (Fig. 4, B and C). MGN3-1 cells also expressed mRNA of insulin receptor (Fig. 4A). Addition of insulin to culture media also suppressed ghrelin secretion from MGN3-1 cell (Fig. 4, D and E). Somatostatin treatment did not affect mRNA expression of either ghrelin or GOAT, even for 24 h incubation (Fig. 4, F and G), whereas insulin significantly suppressed them (Fig. 4, H and I).

Discussion

In this study, we successfully established the first ghrelinoma cell line, MGN3-1 cell. When establishing a cell line for a research tool, the most important thing is how the established cell line keeps its original characteristics. We evaluated the value of MGN3-1 cell by three points: the quantity of ghrelin production, the maintenance of machineries involved in acyl modification and maturation of ghrelin, and the preservation of known *in vivo* regulation of ghrelin secretion.

With regard to the amount of ghrelin production, MGN3-1 cells produced substantial quantities of ghrelin, approximately 5000-fold greater than that produced by

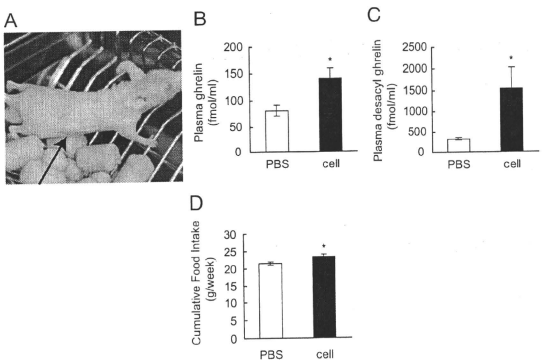

FIG. 3. Transplantation of MGN3-1 cell to nude mouse. A, Macroscopic findings of nude mice injected with MGN3-1 cells. B and C, Plasma ghrelin (B) and desacyl ghrelin (C) levels in nude mice at 4 wk after injection of saline or MGN3-1 cells. D, Cumulative food intake over a week (between 4 and 5 wk after injection) by mice injected with MGN3-1 cells (cell) or PBS. *, $P < 0.05$ in comparison with PBS ($n = 5$).

TT cells (6). It may be reasonable because TT cell is originated from thyroid medullary carcinoma, not from gastric ghrelin-producing cells. As for the machinery of ghrelin acyl modification and maturation, the MGN3-1 cell expressed two key enzymes: GOAT for acylation (16) and PC1/3 for processing (17). We confirmed the activity of GOAT in the MGN3-1 cell by the experiment in which the ratio of ghrelin to total ghrelin levels was decreased by knocking down the GOAT in MGN3-1 cells. Furthermore, addition of octanoic acid significantly increased the N to C ratio of ghrelin in the medium, which is consistent with the *in vivo* finding by Nishi *et al.* (18). We consider these findings important because acyl modification of ghrelin is one of the targets of drug discovery. On the other hand, tricine-SDS PAGE followed by Western blot analysis and reverse-phase HPLC confirmed the maturation of ghrelin in MGN3-1 cells. To provide a concrete evidence for the ability of producing bioactive ghrelin of MGN 3-1 cells, we performed a transplantation of MGN3-1 cells to nude mice, which resulted in the increase in plasma ghrelin levels and the enhancement of food intake in the nude mice. These results indicate that MGN3-1 cell keeps the ability to produce a substantial amount of bioactive ghrelin with normal acyl modification and maturation.

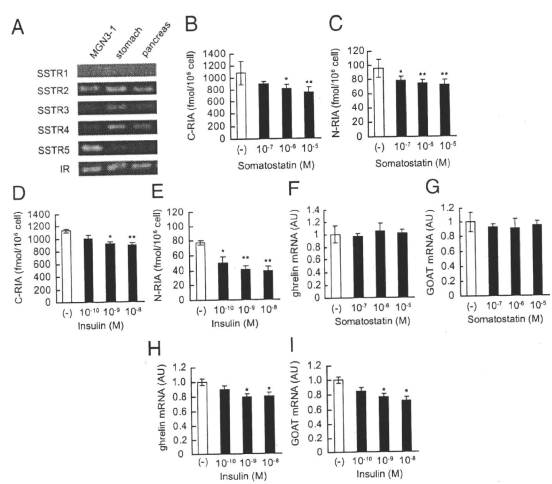

FIG. 4. The effect of somatostatin and insulin on ghrelin secretion and expression in MGN3-1 cells. A, RT-PCR analysis of somatostatin receptor (SSTR) types 1–5 and insulin receptor (IR) mRNA expressions in MGN3-1 cells. B–F, Ghrelin secretion was suppressed when MGN3-1 cells were incubated in DMEM supplemented with somatostatin (B and C) or insulin (D and E) for 4 h ($n = 6$). F–I, Somatostatin did not affect the expression levels of ghrelin (F) and GOAT (G) mRNA in MGN3-1 cell after 24 h incubation, whereas insulin significantly suppressed the expression levels of ghrelin (H) and GOAT (I) mRNA ($n = 6$). AU, Arbitrary unit. *, $P < 0.05$, **, $P < 0.01$ in comparison with (−).

In summary, we have established the first ghrelinoma cell line MGN3-1. The MGN3-1 cell line produces high amounts of bioactive ghrelin with normal acyl modification and maturation and retains physiological regulation by somatostatin. MGN3-1 will be a useful tool for

studying ghrelin production and secretion as well as for screening of ghrelin-modulating drugs.

Acknowledgments

We thank Ms. Chieko Ishimoto and Ms. Chinami Shiraiwa for their excellent technical assistance.

Address all correspondence and requests for reprints to: Hiroshi Iwakura, M.D., Ph.D., 54 Shogoin Kawahara-cho, Sakyo-ku, Kyoto 606-8507, Japan. E-mail: hiwaku@kuhp.kyoto-u.ac.jp.

This work was supported by funds from the Ministry of Education, Culture, Sports, Science, and Technology of Japan and the Ministry of Health, Labor, and Welfare of Japan.

Disclosure Summary: All authors have nothing to declare.

References

1. Kojima M, Hosoda H, Date Y, Nakazato M, Matsuo H, Kangawa K 1999 Ghrelin is a growth-hormone-releasing acylated peptide from stomach. Nature 402:656–660
2. Cummings DE, Purnell JQ, Frayo RS, Schmidova K, Wisse BE, Weigle DS 2001 A preprandial rise in plasma ghrelin levels suggests a role in meal initiation in humans. Diabetes 50:1714–1719
3. Tschöp M, Wawarta R, Riepl RL, Friedrich S, Bidlingmaier M, Landgraf R, Folwaczny C 2001 Post-prandial decrease of circulating human ghrelin levels. J Endocrinol Invest 24:RC19–RC21
4. Tschöp M, Weyer C, Tataranni PA, Devanarayan V, Ravussin E, Heiman ML 2001 Circulating ghrelin levels are decreased in human obesity. Diabetes 50:707–709
5. Ariyasu H, Takaya K, Tagami T, Ogawa Y, Hosoda K, Akamizu T, Suda M, Koh T, Natsui K, Toyooka S, Shirakami G, Usui T, Shimatsu A, Doi K, Hosoda H, Kojima M, Kangawa K, Nakao K 2001 Stomach is a major source of circulating ghrelin, and feeding state determines plasma ghrelin-like immunoreactivity levels in humans. J Clin Endocrinol Metab 86:4753–4758
6. Kanamoto N, Akamizu T, Hosoda H, Hataya Y, Ariyasu H, Takaya K, Hosoda K, Saijo M, Moriyama K, Shimatsu A, Kojima M, Kangawa K, Nakao K 2001 Substantial production of ghrelin by a human medullary thyroid carcinoma cell line. J Clin Endocrinol Metab 86:4984–4990
7. De Vriese C, Delporte C 2007 Autocrine proliferative effect of ghrelin on leukemic HL-60 and THP-1 cells. J Endocrinol 192:199–205
8. De Vriese C, Grégoire F, De Neef P, Robberecht P, Delporte C 2005 Ghrelin is produced by the human erythroleukemic HEL cell line and involved in an autocrine pathway leading to cell proliferation. Endocrinology 146:1514–1522
9. Gutierrez JA, Solenberg PJ, Perkins DR, Willency JA, Knierman MD, Jin Z, Witcher DR, Luo S, Onyia JE, Hale JE 2008 Ghrelin octanoylation mediated by an orphan lipid transferase. Proc Natl Acad Sci USA 105:6320–6325
10. Iwakura H, Ariyasu H, Li Y, Kanamoto N, Bando M, Yamada G, Hosoda H, Hosoda K, Shimatsu A, Nakao K, Kangawa K, Akamizu T 2009 A mouse model of ghrelinoma exhibited activated growth hormone-insulin-like growth factor I axis and glucose intolerance. Am J Physiol Endocrinol Metab 297:E802–E811
11. Iwakura H, Hosoda K, Doi R, Komoto I, Nishimura H, Son C, Fujikura J, Tomita T, Takaya K, Ogawa Y, Hayashi T, Inoue G, Akamizu T, Hosoda H, Kojima M, Kangawa K, Imamura M, Nakao K 2002 Ghrelin expression in islet cell tumors: augmented expression of ghrelin in a case of glucagonoma with multiple endocrine neoplasm type I. J Clin Endocrinol Metab 87:4885–4888
12. Hosoda H, Kojima M, Matsuo H, Kangawa K 2000 Ghrelin and des-acyl ghrelin: two major forms of rat ghrelin peptide in gastrointestinal tissue. Biochem Biophys Res Commun 279:909–913
13. Iwakura H, Ariyasu H, Kanamoto N, Hosoda K, Nakao K, Kangawa K, Akamizu T 2008 Establishment of a novel neuroblastoma mouse model. Int J Oncol 33:1195–1199
14. Iwakura H, Hosoda K, Son C, Fujikura J, Tomita T, Noguchi M, Ariyasu H, Takaya K, Masuzaki H, Ogawa Y, Hayashi T, Inoue G, Akamizu T, Hosoda H, Kojima M, Itoh H, Toyokuni S, Kangawa K, Nakao K 2005 Analysis of rat insulin II promoter-ghrelin transgenic mice and rat glucagon promoter-ghrelin transgenic mice. J Biol Chem 280:15247–15256
15. Akamizu T, Shinomiya T, Irako T, Fukunaga M, Nakai Y, Kangawa K 2005 Separate measurement of plasma levels of acylated and desacyl ghrelin in healthy subjects using a new direct ELISA. J Clin Endocrinol Metab 90:6–9
16. Yang J, Brown MS, Liang G, Grishin NV, Goldstein JL 2008 Identification of the acyltransferase that octanoylates ghrelin, an appetite-stimulating peptide hormone. Cell 132:387–396
17. Zhu X, Cao Y, Voogd K, Voogd K, Steiner DF 2006 On the processing of proghrelin to ghrelin. J Biol Chem 281:38867–38870
18. Nishi Y, Hiejima H, Hosoda H, Kaiya H, Mori K, Fukue Y, Yanase T, Nawata H, Kangawa K, Kojima M 2005 Ingested medium-chain fatty acids are directly utilized for the acyl modification of ghrelin. Endocrinology 146:2255–2264
19. Shimada M, Date Y, Mondal MS, Toshinai K, Shimbara T, Fukunaga K, Murakami N, Miyazato M, Kangawa K, Yoshimatsu H, Matsuo H, Nakazato M 2003 Somatostatin suppresses ghrelin secretion from the rat stomach. Biochem Biophys Res Commun 302:520–525
20. Silva AP, Bethmann K, Raulf F, Schmid HA 2005 Regulation of ghrelin secretion by somatostatin analogs in rats. Eur J Endocrinol 152:887–894
21. Norrelund H, Hansen TK, Orskov H, Hosoda H, Kojima M, Kangawa K, Weeke J, Moller N, Christiansen JS, Jorgensen JO 2002 Ghrelin immunoreactivity in human plasma is suppressed by somatostatin. Clin Endocrinol (Oxf) 57:539–546
22. Broglio F, Koetsveld Pv P, Benso A, Gottero C, Prodam F, Papotti M, Muccioli G, Gauna C, Hofland L, Deghenghi R, Arvat E, Van Der Lely AJ, Ghigo E 2002 Ghrelin secretion is inhibited by either somatostatin or cortistatin in humans. J Clin Endocrinol Metab 87:4829–4832
23. Sugino T, Yamaura J, Yamagishi M, Kurose Y, Kojima M, Kangawa K, Hasegawa Y, Terashima Y 2003 Involvement of cholinergic neurons in the regulation of the ghrelin secretory response to feeding in sheep. Biochem Biophys Res Commun 304:308–312
24. Broglio F, Gottero C, Van Koetsveld P, Prodam F, Destefanis S, Benso A, Gauna C, Hofland L, Arvat E, van der Lely AJ, Ghigo E 2004 Acetylcholine regulates ghrelin secretion in humans. J Clin Endocrinol Metab 89:2429–2433
25. Grinspoon S, Miller KK, Herzog DB, Grieco KA, Klibanski A 2004 Effects of estrogen and recombinant human insulin-like growth factor-I on ghrelin secretion in severe undernutrition. J Clin Endocrinol Metab 89:3988–3993
26. Koutkia P, Canavan B, Breu J, Johnson ML, Grinspoon SK 2004 Nocturnal ghrelin pulsatility and response to growth hormone secretagogues in healthy men. Am J Physiol Endocrinol Metab 287:E506–E512
27. Basa NR, Wang L, Arteaga JR, Heber D, Livingston EH, Taché Y 2003 Bacterial lipopolysaccharide shifts fasted plasma ghrelin to postprandial levels in rats. Neurosci Lett 343:25–28
28. Murdolo G, Lucidi P, Di Loreto C, Parlanti N, De Cicco A, Fatone C, Fanelli CG, Bolli GB, Santeusanio F, De Feo P 2003 Insulin is required for prandial ghrelin suppression in humans. Diabetes 52:2923–2927
29. Saad MF, Bernaba B, Hwu CM, Jinagouda S, Fahmi S, Kogosov E, Boyadjian R 2002 Insulin regulates plasma ghrelin concentration. J Clin Endocrinol Metab 87:3997–4000

Relevant use of Klotho in FGF19 subfamily signaling system in vivo

Ken-ichi Tomiyama[a,b,1], Ryota Maeda[a,b,1], Itaru Urakawa[c], Yuji Yamazaki[c], Tomohiro Tanaka[a,b], Shinji Ito[a,b], Yoko Nabeshima[a,b], Tsutomu Tomita[d], Shinji Odori[d], Kiminori Hosoda[d], Kazuwa Nakao[d], Akihiro Imura[a,b], and Yo-ichi Nabeshima[a,b,2]

[a]Department of Pathology and Tumor Biology, Graduate School of Medicine, Kyoto University, Sakyo-Ku, Kyoto 606-8501, Japan; [c]Pharmaceutical Research Laboratories, Kyowa Hakko Kirin Company, Ltd., Takasaki, Gunma 370-1295, Japan; [b]Core Research for Evolutional Science and Technology, Japan Science and Technology Corporation, Kawaguchi-shi, Saitama 332-0012, Japan; and [d]Department of Medicine and Clinical Science, Graduate School of Medicine, Kyoto University, Sakyo-Ku, Kyoto 606-8501, Japan

Communicated by Yoshito Kaziro, Kyoto University, School of Medicine, Kyoto, Japan, December 9, 2009 (received for review September 28, 2009)

α-Klotho (α-Kl) and its homolog, β-Klotho (β-Kl) are key regulators of mineral homeostasis and bile acid/cholesterol metabolism, respectively. FGF15/ humanFGF19, FGF21, and FGF23, members of the FGF19 subfamily, are believed to act as circulating metabolic regulators. Analyses of functional interactions between α- and β-Kl and FGF19 factors in wild-type, *α-kl*$^{-/-}$, and *β-kl*$^{-/-}$ mice revealed a comprehensive regulatory scheme of mineral homeostasis involving the mutually regulated positive/negative feedback actions of α-Kl, FGF23, and 1,25$(OH)_2$D and an analogous regulatory network composed of β-Kl, FGF15/humanFGF19, and bile acids that regulate bile acid/cholesterol metabolism. Contrary to in vitro data, β-Kl is not essential for FGF21 signaling in adipose tissues in vivo, because (*i*) FGF21 signals are transduced in the absence of β-Kl, (*ii*) FGF21 could not be precipitated by β-Kl, and (*iii*) essential phenotypes in *Fgf21*$^{-/-}$ mice (decreased expressions of *Hsl* and *Atgl* in WAT) were not replicated in *β-kl*$^{-/-}$ mice. These findings suggest the existence of Klotho-independent FGF21 signaling pathway(s) where undefined cofactors are involved. One-to-one functional interactions such as α-Klotho/FGF23, β-Klotho/FGF15 (humanFGF19), and undefined cofactor/FGF21 would result in tissue-specific signal transduction of the FGF19 subfamily.

bile acid | cholesterol | mineral homeostasis | Cyp genes | energy source

The physiological roles of the Klotho family have remained puzzling since the original mutant mouse was developed (1). α-Kl deficiency in mice led to a characteristic phenotype resembling premature aging symptoms in human (1). Thereafter, we found that the overproduction of 1,25$(OH)_2$D and altered mineral-ion homeostasis are the major cause of these premature aging-like phenotypes observed in *α-kl*$^{-/-}$ mice, because the lowering of 1,25$(OH)_2$D activity by dietary restriction (a regimen in which *α-kl*$^{-/-}$ mice are fed a vitamin D–deficient diet) (2) is able to rescue the premature aging–like phenotypes and enable *α-kl*–deficient mice to survive normally without obvious abnormalities. Recently we have reported that α-Kl interacts with fibroblast growth factor 23 (FGF23) in kidney and plays an essential role in maintaining serum 1,25$(OH)_2$D levels by regulation of key active vitamin D–metabolizing enzymes, 1α-hydroxylase (Cyp27b1), and 24-hydroxylalse (Cyp24) (3). We also found that α-Kl binds to Na^+,K^+-ATPase in choroid plexus, parathyroid glands, and the distal convoluted tubules (DCT) of the kidney where extracellular calcium concentration is coordinately regulated (4). In these tissues, Na^+,K^+-ATPase activity is controlled in an α-Kl–dependent manner for transepithelial calcium transport in the choroid plexus and DCT, and for regulated PTH secretion in the parathyroid glands. By associating with both Na^+,K^+-ATPase and circulating FGF23, α-Kl plays a multifunctional role in α-Kl expressing tissues to regulate calcium and phosphate concentrations in vivo. This led to the concept that α-Kl is a regulator that integrates mineral homeostasis (5).

We next identified *β-kl*, which shares structural identity and characteristics with *α-kl* (6). β-Kl is predominantly expressed in the liver, pancreas, and adipose tissues (6) distinct from α-Kl expressing tissues (1, 2). To understand the biological role(s) of β-Kl, we generated a mouse line lacking *β-kl* (7). Although there were no gross abnormalities in the appearance of *β-kl*$^{-/-}$ mice, these mice exhibited an altered metabolism of bile acids, a group of structurally diverse molecules that are primarily synthesized in the liver from cholesterol, promote absorption of dietary lipids in the intestine, and stimulate biliary excretion of cholesterol (8). The enterohepatic circulation of bile acids is regulated largely in hepatocytes where bile acid biosynthesis is regulated by rate-limiting enzymes; cholesterol 7α-hydroxylase (Cyp7a1) and sterol 12α-hydroxylase (Cyp8b1) (8). Bile acids and oxysterols act as ligands to nuclear receptors regulating the expression of important genes in cholesterol homeostasis (9). Particularly, bile acids bind to the promoter region of the farnesoid X receptor (FXR), which induces transcription of small heterodimer partner (SHP), a negative regulator of Cyp7a1 and Cyp8b1, resulting in suppression of bile acids synthesis in a negative feedback manner (9).

Simultaneously, Inagaki et al. reported that FGF15 dramatically suppresses expression of Cyp7a1 through a gut–liver signaling pathway that is different from the FXR/SHP-mediated negative feedback system (10). Moreover, the association of bile acids with FXR leads to the increase of *Fgf15* expression in intestine, resulting in repression of Cyp7a1 in the liver. Importantly, this negative feedback effect was not observed in *Fgf15*$^{-/-}$ and *Fgfr4*$^{-/-}$ mice, and highlighted a concept that the binding of FGF15 with FGFR4 is involved in a second negative feedback system in bile acid metabolism. Taken together, analogous to the role of α-Kl in FGF23/FGFR1-mediated signal transduction, it was hypothesized that β-Kl plays a critical role in FGF15/FGFR4 mediated negative feedback regulation of *Cyp7a1* and *Cyp8b1* expression in the liver (11).

The mammalian FGF family currently consists of 22 members subdivided into seven subfamilies based on their structural similarity and modes of action (12). Most FGFs play an important role as paracrine factors regulating cell growth, regeneration, differentiation, and morphogenesis (13). However, it has been established that members of the FGF-19 subfamily, which also includes FGF21 and FGF23, differ in two important aspects from other FGF proteins. First, they have no or very small mitotic

Author contributions: Y.-i.N. designed research; K.-i.T., R.M., I.U., Y.Y., T. Tanaka, S.I., Y.N., and S.O. performed research; T. Tomita, K.H., K.N., and A.I. analyzed data; and A.I. and Y.-i.N. wrote the paper.

The authors declare no conflict of interest.

Freely available online through the PNAS open access option.

[1]K.-i.T. and R.M. contributed equally to this work.

[2]To whom correspondence should be addressed. E-mail: nabemr@lmls.med.kyoto-u.ac.jp.

This article contains supporting information online at www.pnas.org/cgi/content/full/0913986107/DCSupplemental.

www.pnas.org/cgi/doi/10.1073/pnas.0913986107

effects; and second, they exert their action via systemic, hormone-like effects as metabolic regulators. In fact, human FGF19 (hFGF19) and its murine ortholog FGF15, as well as FGF23, are secreted from ileal enterocytes and bone, respectively, and then circulate in the bloodstream to target tissues (12–14). The third member, FGF21 is predominantly synthesized in the liver (15) and has beneficial effects on several metabolic parameters in different animal models of obesity; recently, FGF21 has been postulated to be a newly found regulator of glucose metabolism through induction of glucose transporter 1 (GLUT 1) (16).

As first shown for FGF23 and subsequently for FGF19, FGF21 has been predicted to require a specific cofactor for its binding to a certain type of FGFR and subsequent activation of FGF21/FGFR signaling pathway. β-Kl has been reported as a candidate cofactor essential for bioactivity of FGF21 in in vitro studies (16–22). However, these have not been confirmed in in vivo studies. It is particularly important to examine (*i*) whether FGF21 signal transduction is abolished in *β-kl*$^{-/-}$ mice and (*ii*) whether the phenotypes of *β-kl*$^{-/-}$ mice significantly overlap with those of *Fgf21*-deficient mice (*Fgf21*$^{-/-}$) (23, 24).

Recent advances in understanding the signaling of FGF19 subfamilies have mainly been based on conventional in vitro experiments (13, 17, 19, 22), whereas in vivo verification of the association of FGF ligands and FGF receptor or of FGF ligands and Klotho family proteins, as well as the signal transduction (phosphorylation) cascades triggered by FGF 19 subfamilies have yet to be confirmed.

In the present study, we demonstrate the first manifest evidence revealing that whereas α-Kl and β-Kl are required for FGF23 and FGF15/hFGF19-mediated signaling pathways in vivo, respectively, β-Kl appears not to be essential for FGF21-mediated signal transduction in vivo.

Results

α-Kl–Dependent Vitamin D Regulation by FGF23. FGF23 is derived from bone and is essential for maintaining phosphate homeostasis and regulation of vitamin D metabolism. In WT mice, administration of hFGF23 results in remarkable suppression of serum 1,25-dihydroxyvitamin D [1,25$(OH)_2$D] through the repression of *Cyp27b1* and induction of *Cyp24* in the kidney. As we previously reported, serum concentrations of 1,25$(OH)_2$D in both *α-kl*$^{-/-}$ and *Fgf23*$^{-/-}$ mice were remarkably higher than that of WT mice (2, 25). Intriguingly, serum FGF23 in *α-kl*$^{-/-}$ mice was >8,000-fold that of WT mice (Fig. 1*A*). To analyze how α-Kl and FGF23 coordinately regulate vitamin D metabolism in the kidney, we analyzed the interactive actions of FGF23 and α-Kl in vivo. The FGFs used in these experiments (hFGF23, hFGF19, hFGF21) were prepared from CHO cell culture media, and their activities were estimated by measuring *Egr-1*-promotor directed Luciferase activities using Peak rapid cells with or without exogenous expression of *α-kl* or *β-kl* (Fig. S1). Furthermore the activity of hFGF21 was confirmed by up-regulation of *Glut1* mRNA in 3T3-L1 adipocyte. To minimize the effects of hypervitaminosis D, a major cause of the abnormalities observed in *α-kl*$^{-/-}$ mice, we used *α-kl*$^{-/-}$ mice fed with a vitamin D–deficient diet, in which serum 1,25$(OH)_2$D levels were normal and consequently most of the premature aging–like phenotypes were alleviated (2).

hFGF23 administration induced a significant decrease in serum 1,25$(OH)_2$D levels in WT mice, whereas no effect was observed in *α-kl*$^{-/-}$ mice (Fig. 1*B*). Consistently, in WT kidneys injected with hFGF23, *Cyp27b1* expression was reduced >13-fold, whereas *Cyp24* expression was induced >5-fold (Fig. 1 *C* and *D*). However, no significant effect of hFGF23 was found on the expression of *Cyp27b1* and *Cyp24* in *α-kl*$^{-/-}$ mice. These results offer direct evidence that α-Kl is essential for FGF23-derived repression of *Cyp27b1* and induction of *Cyp24* in vivo. In addition, we found that the administration of hFGF23 resulted in down-regulation of α-Kl expression (Fig. 1*E*), probably because α-Kl is a target of FGF23 signal transduction and/or because of a secondary effect of decreased 1,25$(OH)_2$D, an inducer of α-Kl gene expression (2). These data implicate an elaborate mutual negative feedback system composed of α-Kl, FGF23, and 1,25$(OH)_2$D in mineral-ion maintenance (Fig. 5*A*).

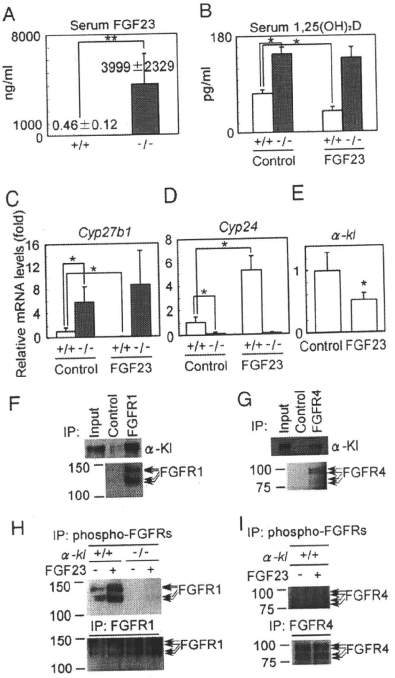

Fig. 1. FGF23 is dependent on α-Kl for regulation of vitamin D synthesis in kidney (*A–E*). (*A*) Serum concentrations of FGF23 in WT and *α-kl*$^{-/-}$ were measured by ELISA. WT (*open bars*) and *α-kl*$^{-/-}$ (*filled bars*) mice (n = 4/group) were injected with recombinant hFGF23 (0.2 mg/kg) or PBS control. Mice were killed 4 h after injection, and serum concentrations of 1,25$(OH)_2$D (*B*) were measured. *Cyp27b1* (*C*), *Cyp24* (*D*), and *α-kl* (*E*) mRNA levels in kidney were analyzed by RT–quantitative PCR. In this and all other figures, error bars represent mean ± SD and are plotted as fold change. Data were derived from 8- to 10-week-old male mice on vitamin D–deficient diets. *$P < 0.05$; **$P < 0.01$. FGFR1 binds to α-Kl and is phosphorylated by FGF23 in the kidney (*F–I*). (*F*) Kidney lysates were precipitated with anti-FGFR1 antibody or with control IgG. Input is 0.01% of the kidney whole extract used for the immunoprecipitation. (*G*) Kidney lysates were precipitated with anti-FGFR4 antibody or with control IgG. Input is 0.2% of the kidney whole extract used for the immunoprecipitation. (*H*) The kidney lysates of WT and *α-kl*$^{-/-}$ mice were immunoprecipitated with the anti-phospho-FGFRs or the anti-FGFR1 antibody. The immunoprecipitates were separated by SDS/PAGE and blotted with anti-FGFR1 antibody. (*I*) Kidney lysates of WT mice were immunoprecipitated with the anti–phospho-FGFRs or the anti-FGFR4 antibody and then blotted with anti-FGFR4 antibody.

α-Kl–Dependent FGFR1 Phosphorylation by FGF23 in Vivo. Generally FGFs can bind to and activate cell surface tyrosine kinase FGF receptors and transduce signals to downstream molecules including MAP kinase (26). The FGF receptor family consists of

four members, FGFR1–4. With the exception of FGFR4, splicing variants in the third Ig-like domain (IIIb and IIIc types) have been identified for each member (12, 26). Recently, it has been reported that α-Kl binds to FGFRs in cultured cells (19) and converts the canonical FGFR1(III)c to a receptor specific for FGF23 (3). We therefore tested whether the above observations were valid in vivo. We first examined the interactions between α-Kl and FGFR1, and α-Kl and FGFR4 in the kidney. As observed in in vitro experiments, α-Kl was coprecipitated not only with FGFR1 but also with FGFR4 in the kidney (Fig. 1*F* and *G*). We then investigated whether these two receptors are activated by hFGF23 in the kidney (procedures are as in *SI Text* and Fig. S2). In WT mice, FGFR1 was activated in the kidney 10 min after injection of hFGF23 (Fig. 1*H*). In contrast, phosphorylation of FGFR4 was not detectable even after the injection of hFGF23 (Fig. 1*I*), suggesting that FGFR4 is not a major receptor responsible for FGF23 signaling in the kidney. As expected, we could not detect phosphorylation of FGFR1 in the kidney of α-$kl^{-/-}$ mice even after hFGF23 injection (Fig. 1*H*). In summary, we concluded that FGFR1 is preferentially activated by FGF23 in a α-Kl–dependent manner in the kidney.

β-Kl–Dependent Bile Acid Regulation by FGF15. Because the unusually elevated expression of Cyp7a1 was observed not only in β-$kl^{-/-}$ mice (7) but also in *Fgf15*$^{-/-}$ and *Fgfr4*$^{-/-}$ mice (10, 27), we predicted that β-Kl was involved in FGF15/FGFR4-signaling system. Based on studies in cultured cells, it was recently proposed that β-Kl is necessary for FGF15/hFGF19-mediated signal transduction in the liver (18, 22). To confirm this hypothesis in vivo, we first measured the mRNA levels of *Fgf15* in the terminal ileum of WT and β-$kl^{-/-}$ mice. Interestingly, *Fgf15* expression levels were ~12-fold increased in β-$kl^{-/-}$ mice compared with those of WT (Fig. 2*A*), analogous to the elevation of FGF23 expression in α-$kl^{-/-}$ mice (Fig. 1*A*). To evaluate the effect of FGF15 in vivo, we administered hFGF19 and analyzed *Cyp7a1* and *Cyp8b1* expression. In WT mice, the expression levels of *Cyp7a1* and *Cyp8b1* 6 h after hFGF19 injection resulted in >100-fold and >10-fold reductions, respectively (Fig. 2 *B* and *C*). These were comparable to findings in a previous study examining FGF15 (10), and thus we concluded hFGF19 could be used to evaluate bile acid regulation in mice. In contrast, the expression levels of *Cyp7a1* and *Cyp8b1* remained elevated in β-$kl^{-/-}$ livers even after the administration of hFGF19 (Fig. 2 *B* and *C*), demonstrating that β-Kl is essential for the negative regulation of Cyp7a1 and Cyp8b1 by FGF15/hFGF19 in vivo. β-Kl-regulated bile acid synthesis by FGF15/hFGF19 is further described in *SI* (Fig. S3).

β-Kl/FGFR4 Coexpression Is Required for FGF15 Signaling in Vivo. To monitor whether FGF15/hFGF19 signals are transduced in tissues other than the liver, we verified *Egr-1* (a zinc-finger transcription factor identified as an immediate-early gene induced by cellular stimulation) mRNA levels in β-Kl–expressing tissues (liver, adipose, pancreas, and salivary gland) as well as several β-Kl–nonexpressing tissues, since hFGF23 administration remarkably increased *Egr-1* expression and induced phosphorylation of 44/42 MAP kinase (ERK1/2) in the kidney where α-Kl is expressed (3). In WT liver, *Egr-1* expression level increased by >120-fold 30 min after hFGF19 administration compared with vehicle (Fig. 2*D*). With respect to other tissues, we observed a faint, but statistically significant *Egr-1* increase in pancreas (>5-fold) and in white adipose tissue (WAT) (~3-fold). Nonetheless, no remarkable changes were observed in other tissues including brown adipose tissue (BAT) and salivary gland despite β-Kl expression. As expected, in β-$kl^{-/-}$ mice injected with hFGF19, no significant induction of *Egr-1* was observed in any of the tissues evaluated (Fig. 2*D*), demonstrating that β-Kl is necessary but not sufficient for FGF15/hFGF19-mediated signal transduction. To address the question of why FGF15/hFGF19 signal is transduced in the liver, pancreas, and WAT, but not in BAT and

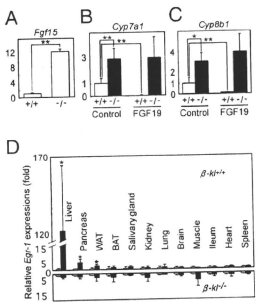

Fig. 2. FGF19 is dependent on β-Kl for regulation of bile acid synthesis in liver (*A–D*). (*A*) mRNA levels of *Fgf15* in terminal ileum in WT and β-$kl^{-/-}$ were measured by RTQ-PCR. WT mice (*open bars*) and β-$kl^{-/-}$ mice (*filled bars*) ($n = 5$/group) were injected with recombinant hFGF19 (1 mg/kg) or control medium. Mice were killed 6 h after injection and *Cyp7a1* (*B*) and *Cyp8b1* (*C*) mRNA levels in liver were measured by RT–quantitative PCR. Data were derived from 14- to 16-week-old male mice on standard diet. Egr-1 induction mediated by FGF19 in liver (*D*). hFGF19 (1 mg/kg) or control medium were injected into WT and β-$kl^{-/-}$ male mice (12–14 weeks old) on standard diet. Thirty minutes after injection, tissues in WT (*Upper*) and β-$kl^{-/-}$ (*Lower*) mice ($n = 4$/group) were excised. *Egr-1* mRNA levels were measured by RT-quantitative PCR. The expression levels of FGF19-injected mice (*filled bars*) and vehicle injected mice (*open bars*) are plotted as fold change. $^*P < 0.05$; $^{**}P < 0.01$.

salivary glands, we profiled the expression of various FGF receptors (FGFRs) in β-Kl–expressing tissues. As reported previously (10), FGFR4 is postulated to be the major receptor responsible for FGF15-mediated signal transduction in the liver. As for the pancreas and WAT, we did observe >2-fold and >6-fold lower *Fgfr4* expression compared with that in the liver, respectively. On the contrary, *Fgfr4* mRNA was not detected in the salivary glands and BAT (Fig. S4). Hence *Egr-1* up-regulation by hFGF19 could be observed in tissues where β-Kl and FGFR4 are coexpressed.

To further demonstrate the contribution of β-Kl in the hepatic FGF15/hFGF19-mediated signaling cascade, we evaluated the phosphorylation of FGFR4 and downstream signaling molecules in vivo using the methods shown in Fig. 1 (Fig. S2 and *SI Text*). β-Kl could be efficiently precipitated by an anti-FGFR4 antibody (Fig. 3*A*) and the phosphorylation of FGFR4 was confirmed after hFGF19 treatment in WT liver (Fig. 3*B*). Unexpectedly, the amount of FGFR4 protein was significantly reduced in livers of β-$kl^{-/-}$ mice (Fig. 3*C*). To obtain an amount of FGFR4 equivalent to that obtained from WT mice, we concentrated the liver lysates from β-$kl^{-/-}$ mice and performed immunoprecipitation (Fig. S2 and *SI Text*). However, we could not detect enhanced activation of FGFR4 in β-$kl^{-/-}$ livers even after injection of hFGF19 (Fig. 3*D*). Consistent with a previous report (18), clear phosphorylation of ERK1/2 was observed in WT livers 10 min after hFGF19 injection, whereas it was undetectable in β-$kl^{-/-}$ livers (Fig. 3*E*), demonstrating that β-Kl is essential for the FGF15/hFGF19 directed activation of FGFR4 and downstream signaling cascade in the liver.

β-Kl Is Not Essential for FGF21-Mediated Signaling in Adipose Tissues. FGF21, a member of the FGF19 subfamily that is synthesized in the liver, has been reported to be a newly found regulator of glucose metabolism (16) and β-Kl has been postulated to be essential for its activity in in vitro studies (17, 20, 21). To examine the possible contribution of β-Kl in the FGF21 signaling system in vivo, we first administered recombinant hFGF21 to WT mice and analyzed *Egr-1* mRNA levels in multiple tissues (Fig. 4*A*). Before its use, we con-

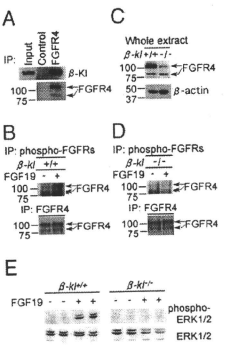

Fig. 3. FGFR4 binds to β-Kl and is phosphorylated by FGF19 in liver. (*A*) Liver lysates were precipitated with anti-FGFR4 antibody or with control IgG. Input is 1% of the liver whole extract used for the immunoprecipitation. The immunoprecipitates were separated by SDS/PAGE and blotted with anti-FGFR4 antibody. (*B*, *D*, and *E*) Ten minutes after injection of hFGF19 or control medium, livers were excised. Liver lysates from WT mice (*B*) and β-$kl^{-/-}$ mice (*D*) were immunoprecipitated with the anti–phospho-FGFRs or the polyclonal anti-FGFR4 antibody. Immunoprecipitates were blotted with anti-FGFR4 antibody. The arrowhead indicates a nonspecific band (Fig. S2). (*C*) Whole liver extracts of WT and β-$kl^{-/-}$ mice were blotted with anti-FGFR4 antibody or anti–β-actin antibody for a loading control. (*E*) Liver lysates from WT and β-$kl^{-/-}$ were immunoblotted with anti-phospho-ERK1/2 or anti-ERK1/2 antibodies ($n = 2$ in each case).

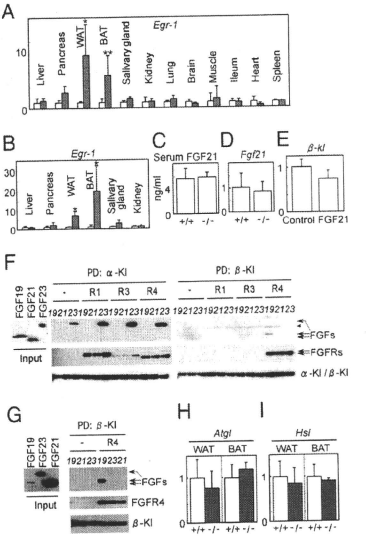

Fig. 4. β-Kl is not essential for FGF21-mediated signaling (*A–I*). Thirty minutes after injection, tissues in WT ($n = 5$/group) (*A*) and β-$kl^{-/-}$ mice ($n = 4$/group) (*B*) were excised. *Egr-1* mRNA levels were measured by RT-quantitative PCR. The expression levels of hFGF21 injected mice (*filled bars*) and vehicle injected mice (*open bars*) mice are plotted as fold change. Data were derived from 7- to 10-week-old male mice on standard diet. (*C*) Serum FGF21 concentrations of WT and β-$kl^{-/-}$ mice ($n = 5$–6/group) were measured by RIA. (*D*) *Fgf21* mRNA levels in livers of WT and β-$kl^{-/-}$ mice ($n = 5$–6/group) were measured by RT-quantitative PCR and are plotted as fold change. Data were derived from 15- to 20-week-old male mice on standard diet. hFGF21 (0.4 mg/kg) or control medium were injected into WT and β-$kl^{-/-}$ mice. (*E*) WT mice were injected with recombinant hFGF21 (0.4 mg/kg) or control medium ($n = 5$/group). Mice were killed 4 h after injection and β-*kl* mRNA levels in WAT were analyzed by RT-quantitative PCR. Data were derived from 10-week-old male mice on standard diet. (*F*) A 15-ng quantity of each FGF was pulled down (PD) by α-/β-Kl in the presence (R1, R3, or R4) or absence (–) of FGFRs. Input was 8% of samples used for the pull-down assay. Samples of pulled down by α-/β-Kl were analyzed by SDS/PAGE and blotted with antibodies (anti-His for FGFs, anti-Human Fc for FGFRs, and anti-GFP for α-/β-Kl). Arrowhead indicates a nonspecific band. (*G*) A 50-ng quantity of FGF19, 150 ng of FGF23, or 500 ng of FGF21 was precipitated by β-Kl in the presence or absence of FGFR4. Input was 1% of samples used for the assay. (*H* and *I*) *hsl* and *atgl* mRNA levels in WAT and BAT were analyzed by RT-quantitative PCR. Data were derived from 9- to 14-week-old female β-$kl^{+/+}$ and β-$kl^{-/-}$ mice ($n = 5$/group). $^*P < 0.05$; $^{**}P < 0.01$.

firmed the biological activity of the synthesized hFGF21. As shown in Fig. S5, our hFGF21 could enhance *Egr1*-derived luciferase reporter expression in a β-Kl–dependent manner at doses that were equivalent to those previously reported (17, 21). Moreover the hFGF21 up-regulated *Glut1* mRNA in 3T3-L1 adipocyte (Fig. S5) (16). Consistent with the in vitro results, in WT mice, *Egr-1* expression levels were significantly up-regulated by ~10-fold in WAT and >6-fold in BAT 30 min after injection of hFGF21 (Fig. 4*A* and Fig. S5). However, administration of hFGF21 also resulted in significant up-regulation of *Egr-1* mRNA levels in WAT and BAT from β-$kl^{-/-}$ mice (Fig. 4*B*). We next analyzed the serum levels of FGF21 and hepatic mRNA levels of *Fgf21* in WT and β-$kl^{-/-}$ mice. Unexpectedly, there was no significant genotype-dependent difference in mean serum protein concentrations of FGF21 nor hepatic *Fgf21* mRNA levels (Fig. 4 *C* and *D*). We also confirmed that β-*kl* expression was not affected by FGF21 administration (Fig. 4*E*). These results suggest that β-Kl is not essential for FGF21-mediated signaling in WAT and BAT. In addition, our prediction was further supported by the following experiments. First, to address the binding properties between β-Kl and FGF21, we performed pull-down assays using recombinant proteins. Although FGF19 was significantly bound by β-Kl in the presence of FGFR4, FGF21 could not be precipitated by β-Kl even with 10 fold amounts of FGF21 (Fig. 4 *F* and *G* and *SI Text*). Second, we compared the phenotypes of $Fgf21^{-/-}$ and β-$kl^{-/-}$ mice. Recently, Hotta et al. developed $Fgf21^{-/-}$ mice and reported that expression levels of hormone-sensitive lipase (*Hsl*) and adipose triglyceride lipase (*Atgl*) in WAT were decreased in $Fgf21^{-/-}$ mice to almost 50% compared with those of WT mice (23). The adipose phenotypes in $Fgf21^{-/-}$ mice may be an outcome of a deficiency in FGF21 signaling. Thus we analyzed the expression levels of these genes in the adipose tissues of β-$kl^{-/-}$ mice. Consequently, in both WAT and BAT, mRNA levels of *Hsl* and *Atgl* were not significantly altered between WT and β-$kl^{-/-}$ mice (Fig. 4 *H* and *I*). These data suggest that β-Kl may not necessarily be involved in the phenotypes observed in FGF21-deficient mice. Taken together, these results provide strong evidence that β-Kl is not essential for FGF21-mediated signaling in WAT and BAT. We therefore asked whether FGF21 signaling might require other unidentified components than β-Kl. We also analyzed *Glut1* mRNA levels 4 h after hFGF21 injection at concentrations that could induce *Egr-1* expression in WAT and BAT, but no apparent induction was observed, suggesting that *Glut1* is not a direct target of FGF21 signaling (28, 29).

Discussion

Various roles of Klotho family members have been reported (18, 22, 30); however, a consensus on the molecular functions of α-Kl

and β-Kl has not been reached. Based on these findings, we propose a comprehensive regulatory scheme of mineral homeostasis that is illustrated by the mutually regulated positive/negative feedback actions of α-Kl, FGF23, and $1,25(OH)_2D$ (Fig. 5*A*). In the present study, we found that FGF23 represses the expression of α-Kl and identified an essential role of α-Kl in FGF23-mediated phosphorylation of FGFR1 in the kidney. This leads to *Cyp27b1* down-regulation and *Cyp24* up-regulation, and results in inhibition of the synthesis of $1,25(OH)_2D$, an active form of vitamin D (3). $1,25(OH)_2D$ has prominent effects on the kidney, intestine, and bone. In the kidney, $1,25(OH)_2D$ activates vitamin D receptor (VDR) by binding to its ligand binding domain and negatively regulates the expression of *Cyp27b1* while positively regulating *Cyp24* and α-Kl expression (2). In the bone, $1,25(OH)_2D$ binds to VDR and induces FGF23 synthesis in osteocytes and osteoblasts (31) in hours/days. In turn, secreted FGF23 suppresses $1,25(OH)_2D$ synthesis and inorganic phosphate reabsorption in the kidney to adjust extracellular mineral concentrations. Collectively, α-Kl, in combination with FGF23, is involved in a signaling cascade that maintains extracellular calcium/phosphate levels within a narrow range.

The roles of β-Kl, FGF15, and FGFR4 in bile acid/cholesterol metabolism are schematically summarized in Fig. 5*B*. Consistent with a previous study (10, 22), i.v. injection of hFGF19 dramatically represses the expression of *Cyp7a1* and *Cyp8b1* and results in the inhibition of bile acid synthesis from cholesterol in WT livers. This suppression of *Cyp7a1* and *Cyp8b1* was not observed in *β-kl*$^{-/-}$ mice. Indeed, phosphorylation of FGFR4 and ERK1/2 was not detected in *β-kl*$^{-/-}$ livers even after hFGF19 administration. Our findings provide conclusive evidence proving the essential role of β-Kl in FGF15/hFGF19-mediated activation of FGFR4 and subsequent signal transduction that regulates bile acid synthesis. Particularly, by binding to FXR, bile acid induces SHP expression in the liver and FGF15 transcription in the terminal ileum. In turn, increased SHP and secreted FGF15 differentially suppress Cyp7a1/Cyp8b1 expression to down-regulate bile acid synthesis (8, 9, 11). In addition, we found mutual negative feedback regulations between β-Kl and FGF15, namely, a decrease in *β-kl* after hFGF19 administration and an increase in *Fgf15* in *β-kl* deficiency. In other words, *β-kl* ablation leads to impaired negative feedback regulation of bile acid metabolism, resulting in the overflow of bile acid pools. Consequently, in the *β-kl*$^{-/-}$ terminal ileum, chronic stimulation by elevated bile acid would lead to an unusual increase in *Fgf15* mRNA. We propose a scheme illustrating the bile acid/cholesterol homeostasis regulated by mutual negative/positive feedback actions of β-Kl, FGF15, and bile acids (Fig. 5*B*).

As shown in Fig. 5, the scheme for bile acid regulation by β-Kl/FGF15 is conceptually analogous to that of vitamin D metabolism, which involves α-Kl and FGF23. Both systems are regulated by the coordination of two types of feedback mechanisms mediated by end-metabolites, $1,25(OH)_2D$ or bile acids, that are in situ negative feedback regulation and target tissue mediated negative feedback loop. In the former pathway, the end-metabolite functions as a nuclear receptor ligand and negatively feeds back by repressing the expression of key regulatory enzymes (Cyp27b1 in the kidney or Cyp7a1/Cyp8b1 in the liver) in the relevant metabolic pathway responsible for the generation of end-metabolite itself. In the latter system, the end-metabolite is transported to the target tissue (bone or intestine) from a distal site and enhances the expression of FGF (FGF23 or FGF15) by binding to the nuclear receptor; VDR or FXR. Subsequently, secreted FGF acts as the regulator of a target tissue–mediated negative feedback loop in collaboration with α-Kl or β-Kl. The next question to be addressed is how these two pathways are coordinately involved in the rapid adjustment and long term maintenance of mineral homeostasis and bile acid metabolism.

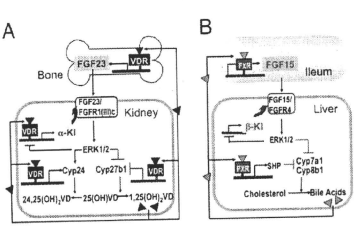

Fig. 5. Schematic representation of α-Kl/FGF23 and β-Kl/FGF15 systems. (*A*) Regulatory network of mineral homeostasis illustrated by the mutual positive/negative feedback actions of α-Kl, FGF23, and $1,25(OH)_2D$. (*B*) Regulatory network of bile acid/cholesterol metabolism represented by the mutual positive/negative feedback actions of β-Kl, FGF15, and bile acids.

In a previous report, we showed that i.v. injection of hFGF23 induces phosphorylation of ERK1/2 and specifically up-regulates the expression of *Egr-1* in the murine kidney (3). Here we demonstrate that α-Kl is required for FGF23 signal transduction in vivo. Likewise, i.v. injection of hFGF19 results in ERK1/2 phosphorylation and up-regulation of *Egr-1* in the liver in a β-Kl–dependent manner. Among β-Kl–expressing organs, significant up-regulation of *Egr-1* was observed in tissues where β-Kl and FGFR4 are coexpressed. Although induction of *Egr-1* in pancreas and WAT are slight, it occurs in a β-Kl–dependent manner. FGF15-mediated signal in pancreas and WAT could therefore be involved in bile acid homeostasis, but its functional importance has yet to be elucidated. Furthermore, the very high *Egr-1* induction in the liver strongly suggests that other elements, in addition to the coexpression of β-Kl and FGFR4, may endow this prominent hepatic signal activation. Recently, several groups have reported that α-Kl and β-Kl can bind to certain types of FGFRs. Those studies report preferences and differences for this binding that might be dependent on assay conditions. α-Kl solely binds to FGFR1(IIIc) in vitro (3), however α-Kl binds to not only FGFR1(IIIc) but also FGFR4 and weakly to FGFR3(IIIc) in cultured cells (30). Even though FGFR4 could precipitate α-Kl in the kidney, activation of FGFR4 by hFGF23 could not be detected. Further studies are required to understand how FGFR(s) is definitively and preferentially used for a particular FGF signal in vivo.

Serum levels of FGF23 and ileac *Fgf15* mRNA expression were intensively increased in *α-kl*$^{-/-}$ and *β-kl*$^{-/-}$ mice, respectively. Furthermore, administrations of hFGF23 and hFGF19 apparently suppressed the expression of *α-kl* and *β-kl*, respectively. In contrast, the serum levels of FGF21 and hepatic *Fgf21* mRNA expression were not increased in *β-kl*$^{-/-}$ mice, and *β-kl* expression was not significantly suppressed by hFGF21 in adipose. Consistent with a previous report that FGF21 induces ERK1/2 phosphorylation specifically in WAT (17), administration of FGF21 to WT mice significantly induced *Egr-1* mRNA expression in WAT and BAT, suggesting that WAT and BAT were the possible target tissues of FGF21. However, surprisingly, remarkable *Egr-1* inductions in WAT and BAT were also observed in *β-kl*$^{-/-}$ mice, indicating that β-Kl is not essential for FGF21 signal transduction in vivo. These in vivo results contrasted with those obtained from in vitro assays, as β-Kl is essential for FGF21-mediated signal transduction in vitro. We reproduced the direct binding of α-Kl and hFGF23 and also confirmed tricomplex formation of β-Kl, hFGF19, and FGFR4 but were unable to detect binding of α-/β-Kl and hFGF21 in our pull-down assay (Fig. 4*G*). Furthermore, we confirmed that the adipose phenotypes in *Fgf21*$^{-/-}$ mice did not overlap with those of *β-kl*$^{-/-}$ mice. This inconsistency leads to a postulation that β-Kl is not necessary for FGF21 signaling.

Currently, β-Kl is believed to be a common player essential for FGF15- and FGF21-mediated signal transduction. However, our present results, together with the data from Hotta et al. (23), do

not support this hypothesis. Possible explanations are that the response found in cultured cells might be caused by: (*i*) an artificial abundance of β-Kl and/or FGF21, (*ii*) peculiar characteristics of the cultured cells used in these experiments, and/or (*iii*) a combination of these two factors (17, 20, 21).

Recent studies have reported that FGF21 stimulates lipolysis in WAT and ketogenesis in the liver (32, 33). However, those results represent the pharmacological effects of sustained FGF21 treatment and thus include consequences that are secondary and indirectly induced by FGF21. We propose a β-Kl–independent response directly triggered by hFGF21 administration. Significant *Egr-1* upregulation in WAT and BAT are indicative that FGF21 mediates lipid metabolism in adipose tissues. The physiological target(s) of FGF21 signaling need to be clarified to understand how FGF21 functions as a regulator of lipid metabolism. Observations using genetic manipulation will lead us to a precise understanding of the roles of the FGF19 subfamily in metabolic homeostasis in vivo.

Materials and Methods

Measurement of Serum Parameters. Blood samples were collected from orbital cavities or hearts under anesthesia and were centrifuged to obtain sera. Serum FGF23 levels were measured by sandwich ELISA (Kainos Laboratory), which can quantify the intact form or FGF23 using human recombinant FGF23 as a standard. Serum $1,25(OH)_2D$ levels were analyzed by SRL, Inc. Serum FGF21 levels were measured by specific RIA (Phoenix Pharmaceuticals, Inc.).

Statistical Analysis. Unless otherwise noted, all values are expressed as mean ± SD. All data were analyzed by the Mann–Whitney *U* test. *P* values less than 0.05 were considered to be statistically significant.

More details are described in *SI Materials and Methods*.

ACKNOWLEDGMENTS. We thank Drs. M. Murata and R.Yu for critical reading of the manuscript and M. Terao and K. Yurugi for support in our experiments. This work was supported Ministry of Education, Science and Culture Grants 19045016 and 21390058 (to A.I.) and 17109004 (to Y-I.N.) and Ministry of Health and Welfare, and Labor Grant H16-genome-005 (to Y-I.N.).

1. Kuro-o M, et al. (1997) Mutation of the mouse Klotho gene leads to a syndrome resembling ageing. *Nature* 390:45–51.
2. Tsujikawa H, Kurotaki Y, Fujimori T, Fukuda K, Nabeshima Y (2003) Klotho, a gene related to a syndrome resembling human premature aging, functions in a negative regulatory circuit of vitamin D endocrine system. *Mol Endocrinol* 17:2393–2403.
3. Urakawa I, et al. (2006) Klotho converts canonical FGF receptor into a specific receptor for FGF23. *Nature* 444:770–774.
4. Imura A, et al. (2007) alpha-Klotho as a regulator of calcium homeostasis. *Science* 316: 1615–1618.
5. Nabeshima Y, Imura H (2008) alpha-Klotho: A regulator that integrates calcium homeostasis. *Am J Nephrol* 28:455–464.
6. Ito S, et al. (2000) Molecular cloning and expression analyses of mouse betaklotho, which encodes a novel Klotho family protein. *Mech Dev* 98:115–119.
7. Ito S, et al. (2005) Impaired negative feedback suppression of bile acid synthesis in mice lacking betaKlotho. *J Clin Invest* 115:2202–2208.
8. Russell DW (2003) The enzymes, regulation, and genetics of bile acid synthesis. *Annu Rev Biochem* 72:137–174.
9. Goodwin B, et al. (2000) A regulatory cascade of the nuclear receptors FXR, SHP-1, and LRH-1 represses bile acid biosynthesis. *Mol Cell* 6:517–526.
10. Inagaki T, et al. (2005) Fibroblast growth factor 15 functions as an enterohepatic signal to regulate bile acid homeostasis. *Cell Metab* 2:217–225.
11. Jones S (2008) Mini-review: Endocrine actions of fibroblast growth factor 19. *Mol Pharm* 5:42–48.
12. Itoh N, Ornitz DM (2004) Evolution of the Fgf and Fgfr gene families. *Trends Genet* 20:563–569.
13. Itoh N, Ornitz DM (2008) Functional evolutionary history of the mouse Fgf gene family. *Dev Dyn* 237:18–27.
14. Nishimura T, Utsunomiya Y, Hoshikawa M, Ohuchi H, Itoh N (1999) Structure and expression of a novel human FGF, FGF-19, expressed in the fetal brain. *Biochim Biophys Acta* 1444:148–151.
15. Nishimura T, Nakatake Y, Konishi M, Itoh N (2000) Identification of a novel FGF, FGF-21, preferentially expressed in the liver. *Biochim Biophys Acta* 1492:203–206.
16. Kharitonenkov A, et al. (2005) FGF-21 as a novel metabolic regulator. *J Clin Invest* 115: 1627–1635.
17. Ogawa Y, et al. (2007) BetaKlotho is required for metabolic activity of fibroblast growth factor 21. *Proc Natl Acad Sci USA* 104:7432–7437.
18. Kurosu H, et al. (2007) Tissue-specific expression of betaKlotho and fibroblast growth factor (FGF) receptor isoforms determines metabolic activity of FGF19 and FGF21. *J Biol Chem* 282:26687–26695.
19. Wu X, et al. (2007) Co-receptor requirements for fibroblast growth factor-19 signaling. *J Biol Chem* 282:29069–29072.
20. Suzuki M, et al. (2008) betaKlotho is required for fibroblast growth factor (FGF) 21 signaling through FGF receptor (FGFR) 1c and FGFR3c. *Mol Endocrinol* 22:1006–1014.
21. Kharitonenkov A, et al. (2008) FGF-21/FGF-21 receptor interaction and activation is determined by betaKlotho. *J Cell Physiol* 215:1–7.
22. Lin BC, Wang M, Blackmore C, Desnoyers LR (2007) Liver-specific activities of FGF19 require Klotho beta. *J Biol Chem* 282:27277–27284.
23. Hotta Y, et al. (2009) Fibroblast growth factor 21 regulates lipolysis in white adipose tissue but is not required for ketogenesis and triglyceride clearance in liver. *Endocrinology* 150:4625–4633.
24. Potthoff MJ, et al. (2009) FGF21 induces PGC-1alpha and regulates carbohydrate and fatty acid metabolism during the adaptive starvation response. *Proc Natl Acad Sci USA* 106:10853–10858.
25. Shimada T, et al. (2004) Targeted ablation of Fgf23 demonstrates an essential physiological role of FGF23 in phosphate and vitamin D metabolism. *J Clin Invest* 113: 561–568.
26. Powers CJ, McLeskey SW, Wellstein A (2000) Fibroblast growth factors, their receptors and signaling. *Endocr Relat Cancer* 7:165–197.
27. Yu C, et al. (2000) Elevated cholesterol metabolism and bile acid synthesis in mice lacking membrane tyrosine kinase receptor FGFR4. *J Biol Chem* 275:15482–15489.
28. Berglund ED, et al. (2009) Fibroblast growth factor 21 controls glycemia via regulation of hepatic glucose flux and insulin sensitivity. *Endocrinology* 150:4084–4093.
29. Xu J, et al. (2009) Fibroblast growth factor 21 reverses hepatic steatosis, increases energy expenditure, and improves insulin sensitivity in diet-induced obese mice. *Diabetes* 58:250–259.
30. Kurosu H, et al. (2006) Regulation of fibroblast growth factor-23 signaling by klotho. *J Biol Chem* 281:6120–6123.
31. Kolek OI, et al. (2005) 1alpha,25-Dihydroxyvitamin D3 upregulates FGF23 gene expression in bone: The final link in a renal-gastrointestinal-skeletal axis that controls phosphate transport. *Am J Physiol Gastrointest Liver Physiol* 289:G1036–G1042.
32. Inagaki T, et al. (2007) Endocrine regulation of the fasting response by PPARalpha-mediated induction of fibroblast growth factor 21. *Cell Metab* 5:415–425.
33. Badman MK, et al. (2007) Hepatic fibroblast growth factor 21 is regulated by PPARalpha and is a key mediator of hepatic lipid metabolism in ketotic states. *Cell Metab* 5:426–437.

Adipose Tissue–Specific Regulation of Angiotensinogen in Obese Humans and Mice: Impact of Nutritional Status and Adipocyte Hypertrophy

Shintaro Yasue[1], Hiroaki Masuzaki[1], Sadanori Okada[1], Takako Ishii[1], Chisayo Kozuka[1], Tomohiro Tanaka[1], Junji Fujikura[1], Ken Ebihara[1], Kiminori Hosoda[1], Akemi Katsurada[2], Naro Ohashi[2], Maki Urushihara[2], Hiroyuki Kobori[2], Naoki Morimoto[3], Takeshi Kawazoe[3], Motoko Naitoh[3], Mitsuru Okada[4], Hiroshi Sakaue[4,5], Shigehiko Suzuki[3] and Kazuwa Nakao[1]

BACKGROUND

The adipose tissue renin–angiotensin system (RAS) has been implicated in the pathophysiology of obesity and dysfunction of adipose tissue. However, neither regulation of angiotensinogen (AGT) expression in adipose tissue nor secretion of adipose tissue–derived AGT has been fully elucidated in humans.

METHODS

Human subcutaneous abdominal adipose tissue (SAT) biopsies were performed for 46 subjects with a wide range of body mass index (BMI). Considering the mRNA level of AGT and indices of body fat mass, the amount of adipose tissue–derived AGT secretion (A-AGT-S) was estimated. Using a mouse model of obesity and weight reduction, plasma AGT levels were measured with a newly developed enzyme-linked immunosorbent assay (ELISA), and the contribution of A-AGT-S to plasma AGT levels was assessed.

RESULTS

A-AGT-S was substantially increased in obese humans and the value was correlated with the plasma AGT level in mice. A-AGT-S and plasma AGT were higher in obese mice, whereas lower in mice with weight reduction. However, the AGT mRNA levels in the liver, kidney, and aorta were not altered in the mouse models. In both humans and mice, the AGT mRNA levels in mature adipocytes (MAs) were comparable to those in stromal-vascular cells. Coulter Multisizer analyses revealed that AGT mRNA levels in the MAs were inversely correlated with the average size of mature adipocytes.

CONCLUSIONS

This study demonstrates that adipose tissue–derived AGT is substantially augmented in obese humans, which may contribute considerably to elevated levels of circulating AGT. Adipose tissue–specific regulation of AGT provides a novel insight into the clinical implications of adipose tissue RAS in human obesity.

Keywords: *adipocyte size; adipose tissue; angiotensinogen; blood pressure; hypertension; obesity*

Am J Hypertens 2010; **23**:425-431 © 2010 American Journal of Hypertension, Ltd.

Activation of the renin–angiotensin system (RAS) is commonly observed in patients with obesity.[1,2] Angiotensin-converting enzyme (ACE) inhibitors and angiotensin II type 1 receptor (AT1R) blockers ameliorate obesity-related metabolic derangement.[3,4] Of note, Case-J trial demonstrated that a systemic blockade of RAS significantly reduced the incidence of newly occurring type 2 diabetes, notably in obese patients with hypertension.[5] Adipose tissue expresses all components of RAS (angiotensinogen (AGT), renin, ACE, AT1R, and angiotensin II type 2 receptor (AT2R)) in humans and rodents,[1] implicating adipose tissue RAS in the pathophysiology of obesity.

AGT, the only substrate of renin, is expressed in a variety of tissues.[1,2] Besides the liver, adipose tissue has recently been recognized as a considerable source of AGT.[1] A previous study demonstrated that transgenic overexpression of AGT exclusively in adipose tissue augmented circulation level of AGT and rescued hypotension and leanness seen in AGT knockout mice.[6] This observation indicates that adipose tissue–derived AGT contributes to circulating AGT level and resultant pathophysiology

[1]Department of Medicine and Clinical Science, Kyoto University Graduate School of Medicine, Kyoto, Japan; [2]Department of Physiology, and Hypertension and Renal Center of Excellence, Tulane University Health Sciences Center, New Orleans, Louisiana, USA; [3]Department of Plastic and Reconstructive Surgery, Kyoto University Graduate School of Medicine, Kyoto, Japan; [4]Division of Diabetes, Digestive, and Kidney Diseases, Department of Clinical Molecular Medicine, Kobe University Graduate School of Medicine, Kobe, Japan; [5]Department of Pharmacology, Kinki University School of Medicine, Sayama, Japan. Correspondence: Hiroaki Masuzaki (hiroaki@kuhp.kyoto-u.ac.jp)

Received 13 September 2009; first decision 3 November 2009; accepted 4 December 2009; advance online publication 7 January 2010. doi:10.1038/ajh.2009.263

of obesity-related metabolic diseases. Although some recent studies demonstrated that expression of adipose AGT is modified by adiposity in humans and rodents,[1,7,8] secretion of adipose tissue–derived AGT *per se* has not been elucidated. Therefore, the extent to which adipose tissue–derived AGT secretion (A-AGT-S) contributes to plasma AGT levels has not been clarified.

In this context, this study was designed to estimate the amount of A-AGT-S, considering the mRNA level of AGT and indices of body fat mass, and explored the potential regulation of A-AGT-S in relation to obesity by performing human adipose tissue biopsies. Furthermore, plasma AGT levels were measured using a newly developed enzyme-linked immunosorbent assay (ELISA),[9,10] and the contribution of A-AGT-S to plasma AGT in mouse models of obesity and weight reduction was assessed.

Although the mechanistic link between adipocyte size and metabolic consequences has long been of research interest,[11,12] the relationship between adipocyte hypertrophy and the expression level of AGT in adipocytes was not fully investigated in humans. Most of the previous studies have employed a histological approach for evaluating adipocyte size.[8,11] However, the distribution of adipocyte diameter is bimodal in humans,[12,13] resulting in limitations in assessing the representative size of adipocytes. In this context, size of mature adipocytes was precisely analyzed using a Coulter Multisizer,[12] and the possible relationship between adipocyte size and AGT mRNA level in adipocytes was explored in humans.

METHODS

Profile of subjects. This study was approved by the ethical committee on human research of Kyoto University Graduate School of Medicine (no. 553). Signed informed consent was obtained from all subjects. A total of 46 Japanese subjects (**Table 1**: 24 men and 22 women; body mass index (BMI): 29 ± 1.0 kg/m^2) were recruited for subcutaneous abdominal adipose tissue (SAT) biopsies. Patients who had received ACE inhibitors, AT1R blockers, thiazolidinediones, insulin, or steroid-related drugs were carefully excluded. Among the group, the serum leptin level was measured in 39 subjects (20 men and 19 women; BMI: 28 ± 1.2 kg/m^2). To examine the relationship between body fat mass and serum leptin level, 55 subjects (BMI: 27 ± 2.1 kg/m^2, range: 15–52) were recruited during the same period.

SAT biopsies. Adipose tissue biopsies were performed before controlling calorie intake and physical activity. SAT (~2 g) was removed from the periumbilical region under local anesthesia (lidocaine 1%). Samples were frozen in liquid nitrogen immediately and stored at −80 °C for total RNA extraction.

Hormone assays and clinical parameters. Blood samples were obtained at 0800 hours after an overnight fast 3 days before the adipose tissue biopsies. Serum leptin levels were measured using RIA (LINCO Research, St Louis, MO).

Real-time PCR. Total RNA was extracted using a QIAGEN RNeasy Kit (QIAGEN Japan, Tokyo, Japan). Complementary DNA was synthesized using an iScript cDNA Synthesis Kit (Bio-Rad, Hercules, CA). The mRNA level was quantified using the TaqMan PCR method with an ABI PRISM 7700 Sequence Detection System (Applied Biosystems, Foster City, CA).[14] The sequences of primers and probes for each gene are summarized in **Table 2**. Values were normalized to that of 18S rRNA (Applied Biosystems).

Obese and weight-losing mouse models. In diet-induced obese (12W DIO, $n = 6$) model experiments, 8-week-old male C57BL/6J mice were housed for 4 weeks on a high-fat/high-sucrose diet (D12493; Oriental Bio-Service, Kyoto, Japan) or regular diet (12W RD, $n = 6$) (F-2; Funahashi, Chiba, Japan). In the weight-losing (14W WL) mouse experiments, 6-week-old male C57BL/6J mice were maintained on a high-fat/high-sucrose diet for 4 weeks, then from 10 weeks of age were subjected to diet substitution from a high-fat/high-sucrose diet to an RD for 4 weeks. In addition, 6-week-old male C57BL/6J mice were maintained on high-fat/high-sucrose diet (14W DIO, $n = 6$) for 8 weeks. Experimental protocol of obese and weight-losing mouse models is schematized in **Supplementary Figure S1** online.

Estimation of A-AGT-S. The amount of A-AGT-S was estimated by multiplying the mRNA level of AGT/g adipose tissue with the weight of body fat mass. Because serum leptin level was tightly correlated with body fat mass,[15] the serum leptin levels were used as a representative index of body fat mass in humans. Estimation of A-AGT-S is schematized in **Supplementary Figure S2** online.

ELISA for AGT. AGT protein was determined using a newly developed ELISA.[9,10]

Cell culture. 3T3-L1 fibroblasts were maintained and differentiated into mature adipocytes.[14] Fully differentiated adipocytes (day 8) were exposed to 10^{-9}, 10^{-8}, or 10^{-7} mol/l dexamethasone for 48 h. Total RNA was extracted from cultured cells using TRIzol Reagent (Invitrogen, Carlsbad, CA). For protein extraction, tissue was homogenized in a radioimmune precipitation (Upstate Cell Signaling Solutions, New York, NY)

Table 1 | Profile of subjects

	n	Mean ± s.e.m.	Range
Age (years)	46	46 ± 2.1	20–74
BMI (kg/m^2)	46	29 ± 1.0	18–52
Waist circumference (cm)	46	93 ± 2.5	63–141
Serum leptin (ng/ml)	39	15 ± 2.2	1.7–68
SBP (mm Hg)	46	131 ± 2.7	94–200
DBP (mm Hg)	46	79 ± 1.5	55–108

BMI, body mass index; DBP, diastolic blood pressure; SBP, systolic blood pressure.

Table 2 | Oligonucleotide sequences for primers and probes

Gene	Forward/reverse primer Probe
Human AGT	5′GGTGGAGGGTCTCACTTTCCA3′/5′ATGGTCAGGTGGATGGTCCG3′ 5′CCCTCAACTGGATGAAGAAACTGTCTCC3′
Human renin	5′GCTATTCAACAGGGACAGTCAG3′/5′TCCGTGACCTCTCCAAACATC3′ 5′AGCCAGGACATCATCACCGTGGGT3′
Human ACE	5′TGCACAGTCTCAACCTGCTG3′/5′CAAGGGCCATCTTCATCAGAAAG3′ 5′TCAGCAGCTCCTAGTTCTTATGCCTTTGGT3′
Human AT1R	5′GGGGCGCGGGTGTATTTG3′/5′TTCAGTAGAAGAGTTGAGAATCATTTTG3′ 5′AGTGTTTGCAACAAATTCGACCCAGGTGA3′
Human AT2R	5′GCTGATTTATGATAACTGCTTTAAACTTC3′/5′GGTGGAGTTGCCCTTCATATTG3′ 5′TCAGCAGCTCCTAGTTCTTATGCCTTTGGT3′
Human adiponectin	5′CCGTGATGGCAGAGATGGCA3′/5′TGAGAAGGGTGAGAAAGGAGATCCAGGT3′ 5′CCGATGTCTCCCTTAGGACCAAT3′
Mice AGT	5′ACACCTACGTTCACTTCCAAG3′/5′CCGAGATGCTGTTGTCCAC3′ 5′ATGAGAGGTTTCTCTCAGCTGCCTGGA3′
Mice renin	5′GCTCCCTGAAGTTGATCATGC3′/5′GTGGGCACCTGGCTACAG3′ 5′CTCTTCTCCTTGGCTCCCAGGGCT3′
Mice ACE	5′TCCCAAAGTATGTGGAGTTCTCC3′/5′TTGTCAGACTCGTATAAGGATCTCC3′ 5′CCCTGCATCCGTGTAGCCATTGAGC3′
Mice AT1aR	5′TACCAGCTCTGCGGCTCTC3′/5′TGCTGTGAGTTATCCAGACAAAATG3′ 5′AGCTCTGCTGCTCTCCCGGACTTAAC3′
Mice AT2R	5′GATGGAGGGAGCTCGGAAC3′/5′TTTAAAGCAGTTATCATAAATCAGCTTAC3′ 5′CACTCCTTAAAATGCAGGCTGAAGTAAGCT3′

The sequences of primers and probes for each gene used in this study are summarized.
AGT, angiotensinogen; ACE, angiotensin-converting enzyme; AT1R, angiotensin II type 1 receptor; AT1aR, angiotensin II type 1a receptor; AT2R, angiotensin II type 2 receptor.

buffer containing protease inhibitors (Complete; Roche, Basel, Switzerland).

Measurement of adipocyte diameter by a Coulter Multisizer. A total of 15 human subjects (5 men and 10 women; age: 51 ± 3.8 years; BMI: 28 ± 2.5 kg/m^2) were analyzed. Stromal-vascular cells and mature adipocytes (MAs) were isolated.[16] Adipocyte size was determined by a Beckman Coulter Multisizer III (Beckman Coulter, High Wycombe, UK).[12] Approximately 8,000 cells were analyzed using a Coulter Multisizer equipped with a 560-μm aperture tube. After collection of pulse sizes, data were expressed as particle diameters and displayed as histograms of counts against diameter, using linear bins and a linear scale for the *x*-axis.[12]

Statistical analyses. Values are expressed as mean ± s.e.m. Values not distributed normally were transformed into a logarithmic (natural logarithm) distribution and were analyzed using Pearson's correlation coefficient. A Student's *t*-test was used to compare the data (Social Research Information, Tokyo, Japan).

RESULTS

AGT mRNA expression and protein synthesis in 3T3–L1 adipocytes and human adipose tissue

Level of mRNA and protein of AGT were measured in lysates and cultured media in 3T3–L1 adipocytes treated with 10^{-9}, 10^{-8}, or 10^{-7} mol/l dexamethasone for 24 h. AGT protein level in lysates and cultured media were strongly correlated with the AGT mRNA level ($r = 0.98$, $P < 0.01$) (see **Supplementary Figure S3a** online) ($r = 0.84$, $P < 0.01$) (see **Supplementary Figure S3b** online).

Relationship between AGT protein/g adipose tissue and AGT mRNA levels in human SAT was also explored ($n = 7$, BMI: 29 ± 0.4 kg/m^2, range 19–48). Consistent with the results in 3T3–L1 adipocytes, AGT protein/g adipose tissue was correlated with the AGT mRNA level in human adipose tissue ($r = 0.77$, $P = 0.04$) (see **Supplementary Figure S3c** online).

Impact of adipose tissue–derived AGT secretion on obesity and blood pressure in humans

The mRNA levels of RAS genes, AGT, renin, ACE, AT1R, and AT2R in human SAT were analyzed. The AGT mRNA level was inversely correlated with BMI ($r = -0.32$, $P = 0.02$) (**Figure 1a**). On the other hand, no correlation was observed between the ACE mRNA level and BMI ($r = 0.08$, $P = 0.63$). The AT1R mRNA level was inversely correlated with BMI ($r = -0.32$, $P = 0.02$). Renin and AT2R mRNA levels were undetectable. The mRNA level of adiponectin was analyzed. No significant correlations were observed between adiponectin mRNA level and BMI ($r = 0.08$, $P = 0.56$) or AGT mRNA level ($r = 0.09$, $P = 0.49$). We also focused our attention on the possibilities of gender differences in AGT gene expression. When divided into two groups (BMI >25 (obese) and BMI <25 (lean)), the differences of AGT mRNA levels by gender were not observed in lean (male $n = 9$:female $n = 12$) and obese (male $n = 15$: female $n = 10$).